PLOS GENETICS

RESEARCH ARTICLE

FXS causing missense mutations disrupt FMRP granule formation, dynamics, and function

Emily L. Starke[1], **Keelan Zius**[1], **Scott A. Barbee**[1,2]*

1 Department of Biological Sciences, University of Denver, Denver, Colorado, United States of America, **2** Molecular and Cellular Biophysics Program, University of Denver, Denver, Colorado, United States of America

* scott.barbee@du.edu

Citation: Starke EL, Zius K, Barbee SA (2022) FXS causing missense mutations disrupt FMRP granule formation, dynamics, and function. PLoS Genet 18(2): e1010084. https://doi.org/10.1371/journal.pgen.1010084

Editor: Gregory P. Copenhaver, The University of North Carolina at Chapel Hill, UNITED STATES

Received: August 20, 2021

Accepted: February 8, 2022

Published: February 24, 2022

Data Availability Statement: All relevant data are within the manuscript and its Supporting Information files.

Funding: We acknowledge funding for this study to SAB from National Institutes of Health (https://www.nih.gov) grant R15MH114019 and from the Assistant Secretary of Defense for Health Affairs Peer Reviewed Medical Program (https://cdmrp.army.mil/prmrp/) grant W81XWH2110026. The funders had no role in study design, data collection and analysis, decision to publish, or preparation of the manuscript.

Abstract

Fragile X Syndrome (FXS) is the most prevalent cause of inherited mental deficiency and is the most common monogenetic cause of autism spectral disorder (ASD). Here, we demonstrate that disease-causing missense mutations in the conserved K homology (KH) RNA binding domains (RBDs) of FMRP cause defects in its ability to form RNA transport granules in neurons. Using molecular, genetic, and imaging approaches in the *Drosophila* FXS model system, we show that the KH1 and KH2 domains of FMRP regulate distinct aspects of neuronal FMRP granule formation, dynamics, and transport. Furthermore, mutations in the KH domains disrupt translational repression in cells and the localization of known FMRP target mRNAs in neurons. These results suggest that the KH domains play an essential role in neuronal FMRP granule formation and function which may be linked to the molecular pathogenesis of FXS.

Author summary

Fragile X Syndrome (FXS) is the most common inherited neurodevelopmental disorder in humans and single gene cause of autism. Most cases of FXS are caused by the complete loss of a single protein (called FMRP). This has made it particularly difficult to understand which of the normal functions of FMRP are disrupted in cases of FXS. Recently, advances in high-throughput sequencing technologies have led to the discovery of patients with severe FXS caused by single mutations in important regions of the FMRP protein. Using a well-characterized FXS model system, we have found that two disease-causing mutations in FMRP disrupt the formation, dynamics, and function of RNA- and protein-containing granules in neurons. These granules have been shown to be involved in the transport of mRNA cargos in axons and dendrites. Disruption of these granules is linked to defects in synaptic development and plasticity. Our results show that two regions of the FMRP protein play a critical role in the control of FMRP granules. These findings suggest the disruption of these processes may be linked to FXS pathogenesis.

Competing interests: The authors have declared that no competing interests exist.

Introduction

Fragile X Syndrome (FXS) is the most common cause of inherited intellectual disability in humans [1]. Typically, FXS is caused by epigenetic silencing of the *FMR1* gene due to a long CGG repeat expansion in the 5'UTR, resulting in hypermethylation of the *FMR1* locus and subsequent transcriptional silencing [2]. This results in loss of expression of the encoded Fragile X Mental Retardation Protein (FMRP), an evolutionarily conserved RNA-binding protein (RBP) that binds to many mRNAs in the mammalian brain. FMRP is best characterized as a translational repressor [3]. In this role, FMRP associates with diverse ribonucleoprotein particles (RNPs) including RNA transport granules, P-bodies (PBs), and stress granules (SGs) [4]. In neurons, FMRP-containing RNA transport granules (hereafter called "FMRP granules") are actively transported in both axons and dendrites [5–8]. These granules carry translationally repressed mRNAs to synapses where they are derepressed in response to synaptic activity. Local translation of critical mRNAs is essential for long-term synaptic plasticity and is defective in FXS [9].

The role of FMRP in translation and mRNA transport in the context of neurons remains enigmatic. In the soma, FMRP binds to translationally repressed target mRNAs and associated RBPs. These RNPs merge and are remodeled to allow for rapid, motor-dependent transport within neurites [10]. FMRP granules belong to a diverse class of membraneless organelles (MLOs) that form through liquid-liquid phase separation (LLSP) [11]. This process is driven by weak, multivalent interactions between protein and RNA components [12,13]. Weak interactions allow MLOs to be highly dynamic and to rapidly assemble and disassemble in response to local signals. In the case of FMRP, posttranslational modification of its C-terminal intrinsically disordered region (IDR) can reversibly control its phase separation *in vitro*, a process that correlates with translational repression [14]. This is an attractive model to explain how FMRP granules might assemble, deliver translationally repressed mRNAs to the synapse, and then regulate their local translation in response to activity. However, it is unclear whether the IDR acts alone or together with structured RBDs to regulate FMRP granules *in vivo*.

Although the most common cause of FXS is loss-of-function, advances in gene sequencing have led to the discovery of FXS-causing missense mutations in the *FMR1* gene [15]. Two mutations located in structured N-terminal RBDs of FMRP and have been functionally characterized [16–21]. The Gly266Glu (G266E) and Ile304Asn (I304N) mutations are in K-homology domains (KH1 and KH2 respectively) which bind to "kissing-complex" tertiary motifs or distinct sequence elements (GACR, ACUK, and WGGA) within target mRNAs [22–24]. The latter are ubiquitous sequences in mammalian transcripts [25]. The analysis of these mutations has begun to uncover novel functions for *FMR1*. For example, both the G266E and I304N disrupt the ability of FMRP to bind to specific target mRNAs and to associate with polysomes suggesting that the KH domains are important for translational regulation [18,26]. However, the precise role these domains play in FMRP granule formation, dynamics, and function in the context of neurons remains unknown.

Studying FMRP function in mammals is genetically complicated due to the presence of two autosomal paralogs, FXR1P and FXR2P, which have some functional redundancy with FMRP [27–29]. In contrast, *Drosophila* has a single *dFmr1* gene and the dFMRP protein shares significant sequence identity with mammalian FMRP, particularly within the RBDs [29]. *Drosophila* FMRP granules are also compositionally like those observed in mammalian neurons [30,31]. Importantly, *Drosophila* has proven to be an excellent model system in which to study FXS because *dFmr1* mutants recapitulate many FXS phenotypes [32]. Here, we have introduced analogous mutations into the KH1 and KH2 domains of dFMRP (G269E and I307N respectively) and examined FMRP granules in *Drosophila* Schneider (S2) cells and primary neurons.

Analysis of these mutants has revealed distinct differences in the requirement for KH1 and KH2 in the formation and dynamics of FMRP granules. Interestingly, both FXS-causing KH mutations result in FMRP granules that are significantly more dynamic. This is in opposition to mutations in other RBPs that drive the formation of solid-like aggregates associated with neurodegenerative disorders. Finally, the KH mutations differentially impact the function of FMRP in translational repression and RNA transport. Our findings provide new biological insight into the normal function of FMRP in cells and neurons and into the specific molecular and cellular processes that are dysregulated in FXS.

Results

The KH domains are required to form FMRP granules in cells

The C-terminal IDR of mammalian FMRP is necessary and sufficient to drive the formation of phase-separated liquid droplets *in vitro* [14]. However, the dependency of the IDR in FMRP granule formation in cells has yet to be elucidated. To address this, we first developed dFMRP deletion and mutant transgenes (Fig 1A). Unless otherwise noted, EGFP was fused to the N-terminus to visualize granules. Overexpression of GFP-tagged wild-type dFMRP (WT-FMRP) in *Drosophila* larval motor neurons (MNs) replicated published results with untagged dFMRP indicating that GFP does not significantly interfere with protein function (S1 Fig) [33].

The C-terminus of dFMRP is predicted to be disordered, indicating it may play an important role in promoting LLPS (Fig 1A). We first transfected *Drosophila* S2R+ cells with WT-dFMRP, $dFMRP_{\Delta IDR}$ (ΔIDR), and $dFMRP_{IDR}$ (IDR) (Fig 1B and 1C). As shown previously, 98% of cells transfected with WT-FMRP form numerous small round granules (Fig 1C and 1D) [34,35]. We found that the IDR alone was sufficient to induce FMRP granules in 65% of transfected cells (Fig 1C and 1D). These granules were morphologically like WT-FMRP albeit less numerous (Fig 1E–1G). Interestingly, the structured N-terminal domain of dFMRP (ΔIDR) was also sufficient to induce granule formation in 26% of cells (Fig 1C and 1D). These granules were less abundant, and many had an amorphic (non-circular) morphology (Fig 1E and 1G). These data suggest that the IDR of dFMRP greatly enhances granule formation.

We speculated that the N-terminal KH1 and KH2 domains may act cooperatively with the IDR to regulate FMRP granule formation. Fusing the KH domains to the IDR (KH+IDR) significantly increased the number of cells containing granules (Fig 1D). These foci were morphologically indistinct from WT-FMRP granules although the number of KH+IDR granules per cell did not increase significantly (Fig 1C and 1E–1G). These data indicate that the propensity to form granules is enhanced by addition of the KH domains to the IDR. However, our results also suggest that additional elements in the N-terminus are likely to be involved in the control of FMRP granule formation.

FXS-causing mutations in the KH domains disrupt granule formation

We next wanted to explore the contribution of the KH domains in FMRP granule formation. The G266E and I304N missense mutations in KH1 and KH2 of hsFMRP are predicted to disrupt the proper folding of each RBD and to disrupt functions of FMRP including mRNA-binding, AMPA receptor trafficking, and polysome association [22,26,36]. To address this, we made analogous point mutations in the KH domains of dFMRP (G269E and I307N), hereafter referred to as KH1* and KH2* (Fig 2A). In contrast to WT-FMRP, overexpression of the GFP-tagged KH1* and KH2* transgenes in larval MNs did not inhibit axon terminal growth at the neuromuscular junction (NMJ) (S1 Fig) [33].

We transfected S2R+ cells with GFP-tagged constructs to determine the impact these mutations had on FMRP granule formation. Interestingly, we observed a $>$ 2-fold decrease in the

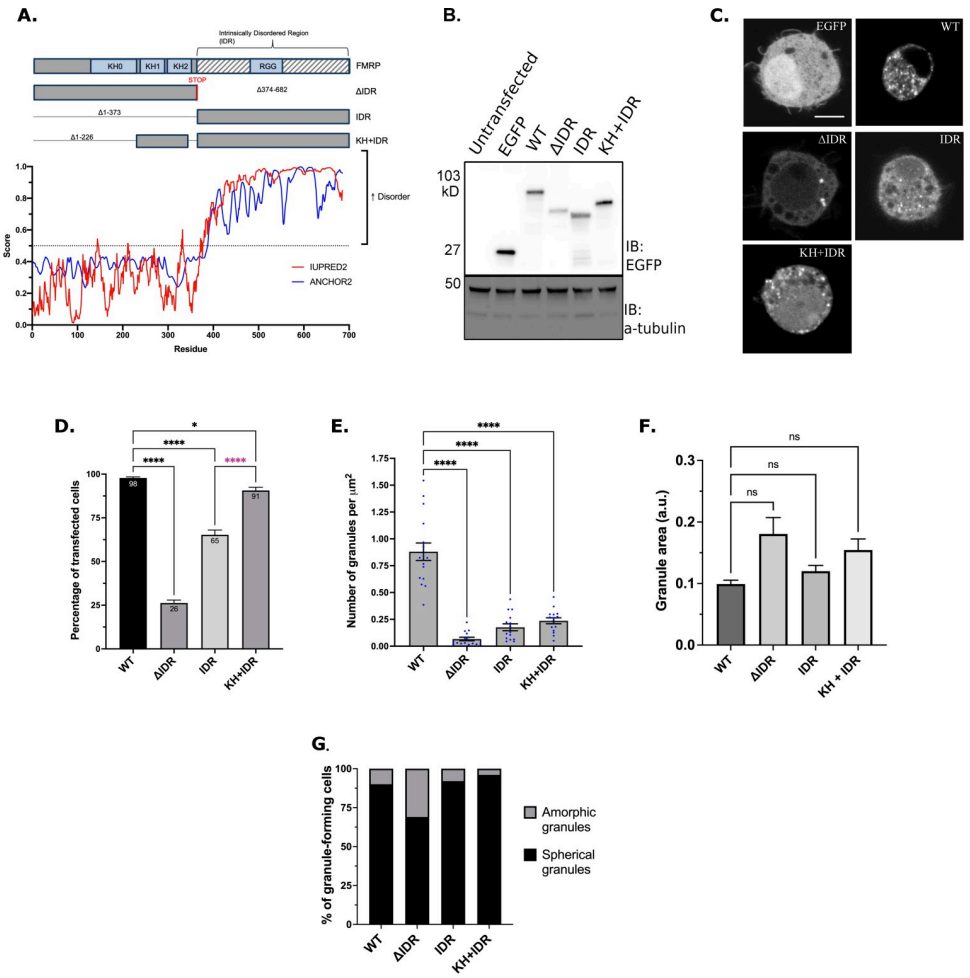

Fig 1. The KH domains and IDR interact to regulate FMRP granule formation. (A) Schematic of dFMRP showing each of the main RBDs in light blue boxes and IDR indicated by grey and white stripes (top). IDR mutants denote amino acid deletions with lines. Both KH1 and KH2 domains are fused to the IDR in the KH+IDR mutant. Disorder plot aligned with the wild-type dFMRP protein show that the C-terminus is entirely disordered as predicted by IUPRED2 and ANCHOR2 [74]. (B) Western blot analysis of EGFP (GFP) and α-tubulin (loading control) protein levels in transfected cells. (C) Representative images of GFP-FMRP mutant granule phenotypes in transfected S2R + cells. Scale bar = 2μm. (D) Percentage of transfected cells forming GFP-FMRP granules. Data are presented as mean ± S.E. of three independent experiments (approximately 100 cells per experiment; one-way ANOVA). (E) Quantification of the number of granules counted within a cell, which was normalized to cell area in μm^2 (mean ± SE; n = 15 cells; Brown-Forsyth test). The data shown for the WT controls in Fig 1E are identical to those shown in Fig 2E. The cells analyzed here are from an independent experiment. (F) Quantification of the relative size of granules (a.u.) in a new experiment (mean ± SE; Kruskal-Wallis test). Number of granules analyzed per genotype was WT = 213 (8 cells), ΔIDR = 44 (14 cells), IDR = 102 (12 cells), KH + IDR = 60 (14 cells). (G) Quantification of the two major morphological phenotypes observed in IDR mutants (n = 100 cells). In D-F, * $p<0.05$; **** $p<0.0001$.

https://doi.org/10.1371/journal.pgen.1010084.g001

ability of cells expressing GFP-tagged KH1* to form granules relative to WT-FMRP, while KH2* had no effect (Fig 2C and 2D). This decrease cannot be explained by a difference in the expression levels of GFP-KH1* (Fig 2B). We also found that the number of granules per cell was significantly reduced by both mutations, although, granules were about twice as abundant in KH2* than KH1* (Fig 2E). Many KH2* granules also had an unusual, often large, amorphic structure while both WT-FMRP and KH1* granules were generally small and round (Fig 2C and 2F–2G). These results suggest that both the KH1 and KH2 mutants alter normal FMRP granule formation. They also suggest that each KH domain control a different aspect of this process.

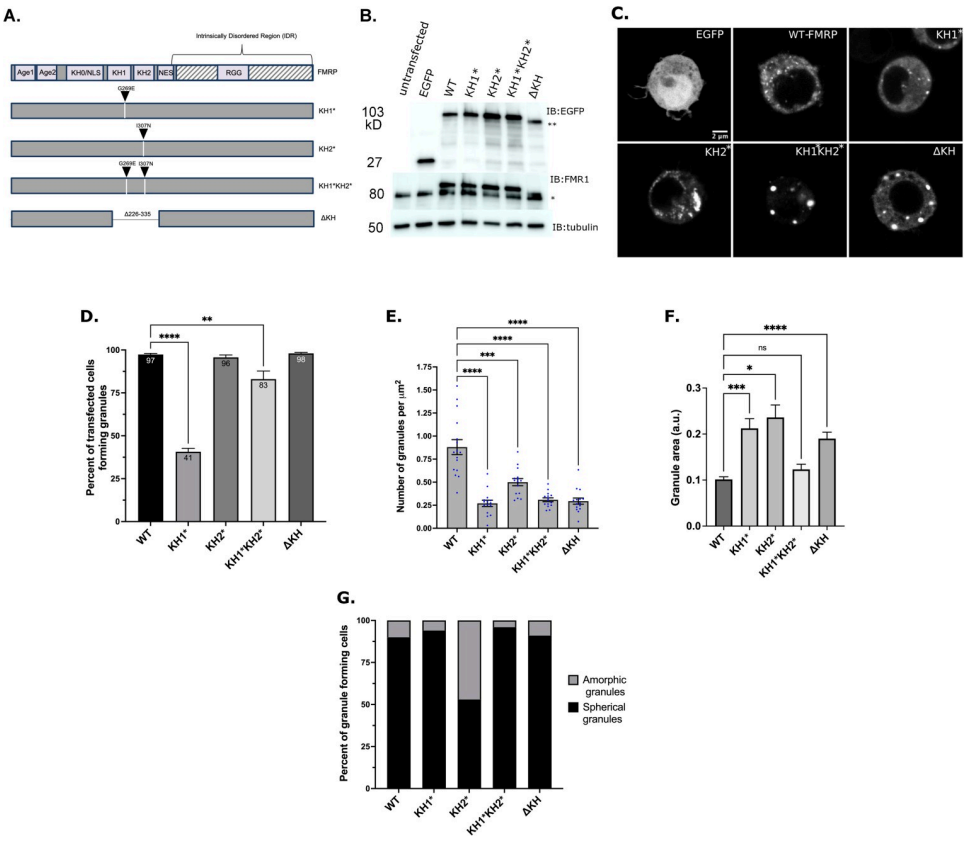

Fig 2. The KH domains differentially regulate FMRP granule formation. (A) Schematic representation of dFMRP variants used in this study. Arrowheads indicate where analogous FXS-causing point mutations were made in dFMRP. Deletion of the KH1 and KH2 domains is annotated with a break in FMRP sequence. (B) Western blot analysis of EGFP (GFP), FMRP, and α-tubulin protein levels in transfected cells. α-tubulin was used as a loading control (* = 80 kDa, ** = 90 kDa). The upper bands on the FMR1 blot are the EGFP:FMRP fusion protein. (C) Representative images of cells transiently transfected with the indicated GFP-tagged FMRP constructs. Scale bar = 2 μm. (D) Percentage of transfected cells forming GFP-FMRP granules. Data are presented as mean ± S.E. (approximately 100 cells per three experiments; one-way ANOVA). (E) Quantification of the number of granules per cell, which was normalized to cell area in μm^2 (mean ± SE; n = 15 cells each; Brown-Forsyth test). The data shown for the WT controls in Fig 2E are identical to those shown in Fig 1E. The cells analyzed are otherwise from an independent experiment. (F) Quantification of the relative size of granules (a.u.) in a new experiment (mean ± SE; Kruskal-Wallis test). Number of granules analyzed was WT = 209 (8 cells), KH1* = 85 (13 cells), KH2* = 127 (15 cells), KH1*KH2* = 110 (14 cells), ΔKH = 118 (15 cells). (G) Quantification of the two major morphological phenotypes observed (n = 100 cells each). In D-F, **p<0.01, ***p<0.001, ****p<0.0001.

https://doi.org/10.1371/journal.pgen.1010084.g002

To examine the collective contribution of both domains, we made a G269E/I307N double mutant (KH1*KH2*) (Fig 2A). Most cells transfected with these constructs were able to form granules (Fig 2C and 2D). As with the individual KH mutants, transfected cells contained fewer granules per cell (Fig 2E). Interestingly, most KH1*KH2* granules that formed in cells were large and round indicating that they are different from those containing WT-FMRP, KH1*, or KH2* (Fig 2C and 2F–2G). KH1*KH2* also partially rescued the granule formation defect see with KH1* alone. This suggests that the negative effect of KH1* requires normal KH2 function. Morphologically these were like a published mutant where both KH domains have been deleted (ΔKH) [34,35]. Together, these data suggest that the KH domains work together to restrict the size and shape of FMRP granules. However, we cannot rule out that the disruption of both KH domains is changing overall protein structure which is causing the formation of aggregates containing GFP-ΔKH and GFP-KH1*KH2* protein.

FXS-causing mutations in the KH domains alter the dynamics of FMRP granules

A defining feature of phase separated RNPs in cells is the ability of components to rapidly shuttle between granules and the cytosol. The driving force underlying this process is multivalent interactions between protein and RNA components [37]. To examine whether the G269E and I307N mutations influenced dFMRP dynamics, we first conducted Fluorescence Recovery After Photobleaching (FRAP) experiments in S2R+ cells. The fluorescent signal of GFP-tagged WT-FMRP recovered to 82% with a $t_{1/2}$ of 21.9s, in agreement with published results (Fig 3C and 3D) [35]. We found that the exchangeable pool of KH1* and KH2* was like WT-FMRP (Fig 3C). However, KH1* and KH2* granules recovered more rapidly ($t_{1/2}$ = 4.3 and 13.1s) suggesting these foci are much more dynamic than WT-FMRP (Fig 3A, 3B and 3D). Collectively, these data indicate that the individual KH mutations decrease the stability of FMRP in the mobile fraction, or the portion of fluorescent molecules capable of diffusing freely in and out of the granule. KH2* granules did recover ~3 fold more slowly that KH1* granules sugging that KH2* are less dynamic. This is supported, in part, by our morphology data showing that KH2* has the tendency to form less liquid-like amorphous structures (Fig 2F). Finally, we examined the effect of removing or disrupting both KH domains. Compared to single mutants, KH1*KH2* significantly reduced dFMRP in the mobile fraction to 66% suggesting a large shift of FMRP into the non-dynamic immobile fraction (Fig 3C). Similar results were observed with the ΔKH mutant, however, recovery time of FMRP in the mobile fraction was significantly increased ($t_{1/2}$ = 98.7s) (Fig 3D). These results further suggest that disruption of both the KH domains may lead to the strengthening of interactions and/or protein aggregation.

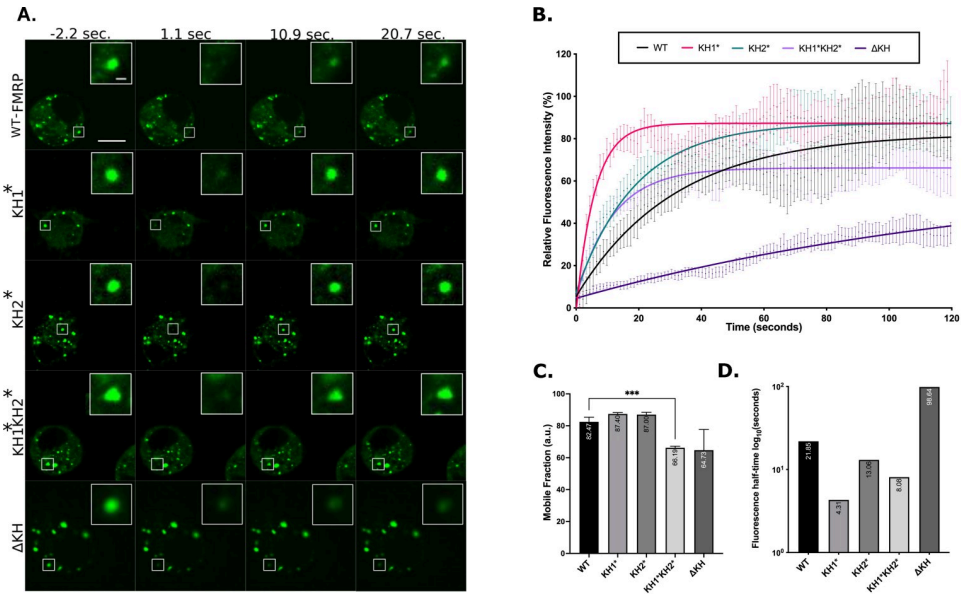

Fig 3. FXS-causing mutants alter FMRP granule dynamics in S2R+ cells. (A) Representative time-lapse FRAP images of FMRP-mutants pre- and post-bleaching. Scale bar in whole cell image = 5μm. Scale bar in zoomed-in granule image = 0.5μm. (B) Fluorescence recovery curves of FMRP-mutants over 120 seconds. Data points are mean ± SE. (C) Mobile fraction of FMRP mutant granules (mean ± SE; Brown-Forsyth test; ***p<0.001). a.u. = arbitrary units. (D) Quantification of the average time in $\log_{10}$ (seconds), for granules to recover to half their final intensity ($t_{1/2}$). For B, C, and D n = 17–21 granules.

https://doi.org/10.1371/journal.pgen.1010084.g003

FXS-causing mutations alter the liquid-like properties of stress granules

In addition to neuronal granules (NGs), FMRP is a component of both SGs and PBs in neurons [4]. Precisely how FMRP interacts with different populations of granules has yet to be elucidated. We hypothesized that mutations in the KH domains might disrupt the association of FMRP with these RNP populations. To study interactions with SGs, we co-transfected S2R + cells with GFP-tagged FMRP constructs and mCherry-tagged Rasputin (Rin), the fly ortholog of G3BP1, a conserved marker for and modulator of SG assembly [38]. In concordance with previous studies, overexpression of Rin induced SG formation in ~20% of unstressed transfected cells (Fig 4A and 4D) [38]. Interestingly, we found that these Rin-positive granules always contained GFP-tagged WT-FMRP and GFP-KH1* always colocalized with Rin (Fig 4A). They were also resistant to treatment with 1,6-hexanediol (1,6-HD), an aliphatic alcohol believed to interfere with weak protein-protein (π-π) and protein-RNA (π-cation) interactions required to form liquid-like MLOs [39] (Fig 4D). As expected, arsenite-induced stress triggered the formation of cytoplasmic SGs (Fig 4B and 4E). Surprisingly, co-transfection with GFP-KH1* or GFP-KH2* significantly reduced the number of cells that formed Rin-positive SGs (Fig 4E; left). Moreover, the SGs that formed in cells co-transfected with KH mutants were more resistant to 1,6-HD treatment then with WT-FMRP (Figs 4E, right, and S2). Together, this suggests that the liquid-like nature of SGs is partially disrupted by the KH mutations.

Mammalian FMRP also accumulates in SGs under conditions of arsenite stress [40]. In concordance with these results, all GFP-tagged dFMRP constructs colocalized strongly with Rin in stressed cells (Fig 4F). The number of cells containing KH mutant granules also increased in stressed cells but those with KH1* and KH1*KH2* were still significantly lower than WT-FMRP (Fig 4G and 4H; left). As with Rin, all KH mutant granules in stressed cells were significantly more resistant to 1,6-HD compared to WT-FMRP (Figs 4H, right, and S2). In the case of the KH1* and KH2* mutants, this was not likely due to the persistence of pre-existing FMRP granules because these nearly disappear in unstressed cells (Fig 4G; right). This further suggest that the liquid-like nature of SGs has been disrupted by the single KH mutants. The presence of KH1*KH2* and ΔKH granules in unstressed cells and their resistance to 1,6-HD treatment provides a third line of evidence suggesting that these mutations are causing FMRP to aggregate.

FXS-causing mutations alter the localization of FMRP to P-bodies

In addition to SGs, FMRP has been shown to colocalize with PB proteins in fly and mammalian neurons [30,31]. Thus, we were next interested in determining if the KH mutants affected the ability of FMRP to interact with HPat/Pat1p, a highly conserved PB protein that colocalizes with FMRP in *Drosophila* neurons [41,42]. To address this, we co-transfected S2R+ cells with GFP-tagged FMRP constructs and immunostained against HPat (Fig 4C). As expected, WT-FMRP overlapped moderately with HPat-positive granules (Fig 4I). In comparison, colocalization was significantly reduced in KH1* and most punctate GFP-KH1* failed to colocalize with punctate HPat (Fig 4C and 4I). In contrast, KH1*KH2* and ΔKH caused the formation of larger granules that strongly colocalized with HPat, suggesting that PB proteins may aggregate in these structures (Fig 4C and 4I). Taken together, these data suggest that the KH domains regulate the association of FMRP with PBs. Based on these results and its propensity to form solid-like aggregates, we excluded ΔKH from subsequent analyses in neurons.

The KH1 domain is required for FMRP granule formation in primary neurons

FMRP granules are important for the regulated trafficking of FMRP and specific RNA cargos in axons and dendrites [5–7,10,43,44]. Based on our results in S2R+ cells, we asked if either of the KH domains played a role in the assembly or dynamics of FMRP granules in neurons. We

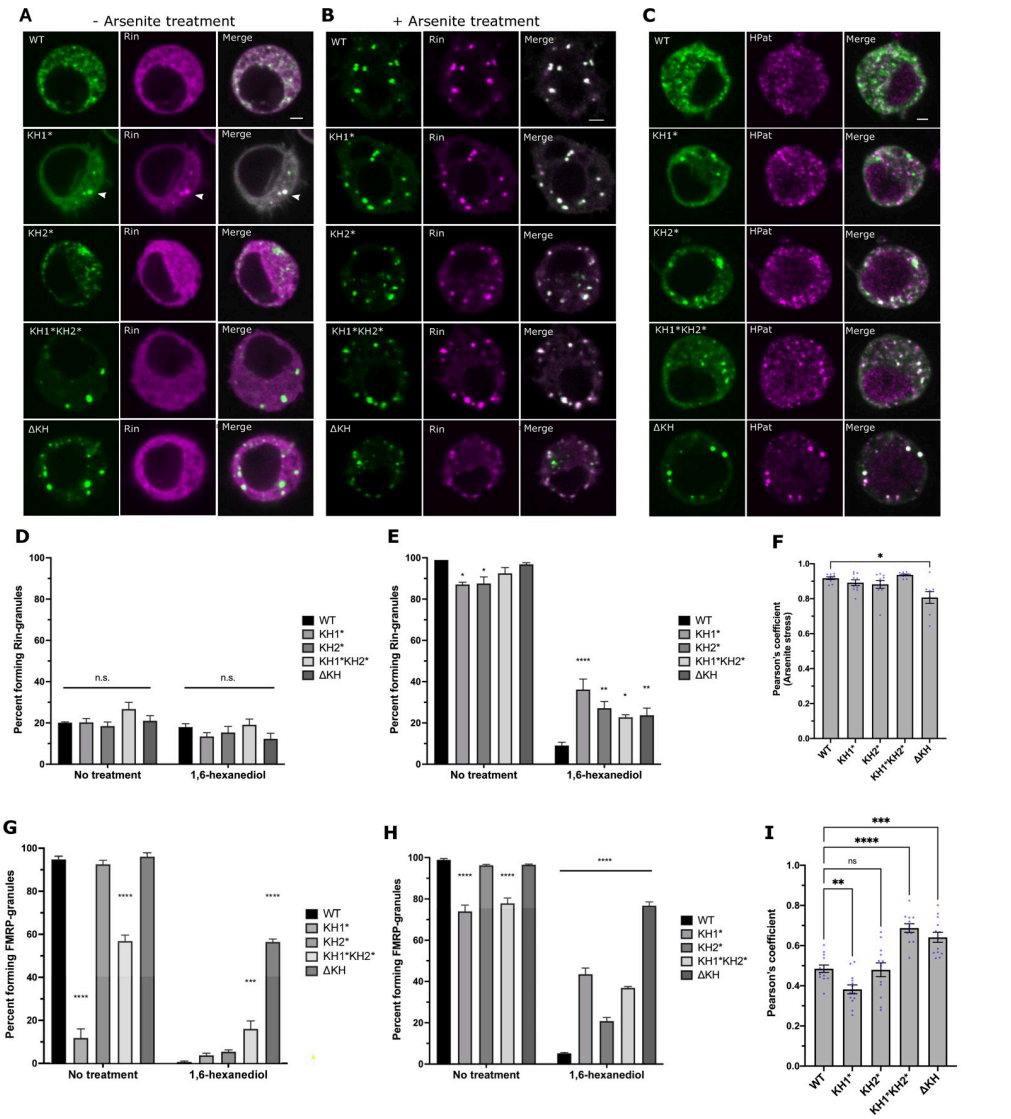

Fig 4. FXS-causing mutations alter SG dynamics and PB association. Representative images of S2R+ cells transfected with GFP-FMRP mutants (green) and Rin-mCherry (magenta) that are either not treated (A) or treated (B) with 0.5mM sodium arsenite for 45 minutes. Scale bars = 2μm. (C) Representative images of the localization of transiently transfected GFP-FMRP mutants immunostained against GFP (green) and HPat (magenta). Scale bar = 2μm. Percent of unstressed (D) or arsenite stressed (E) transfected cells forming Rin-positive SGs with or without 10% 1,6-HD treatment. Comparisons are made to WT-FMRP in each subcategory (mean ± SE; ~100 cells in triplicate; one-way ANOVA). (F) Average Pearson's correlation coefficient between FMRP-mutants and the stress granule marker, Rin, in arsenite treated cells (mean ± SE of 8–10 cells; Brown-Forsyth test). Percentage of unstressed (G) or arsenite stressed (H) transfected cells forming FMRP granules with or without 10% 1,6-HD compared to WT-FMRP (mean ± SE; ~100 cells in triplicate; one-way ANOVA). (I) Average Pearson's correlation coefficient between FMRP-mutants and HPat (mean ± SE of 12–13 cells; one-way ANOVA). In all graphs: * $p<0.05$, $^{**}p<0.01$, $^{***}p<0.001$, $^{****}p<0.0001$.

https://doi.org/10.1371/journal.pgen.1010084.g004

generated inducible GFP-tagged dFMRP transgenic lines. First, we examined fly viability in a $dFmr1^{\Delta 50M}/dFmr1^{\Delta 113}$ (*Δ50/Δ*113) loss-of-function genetic background when transgenes were expressed in larval motor neurons (*C380-Gal4*, *cha-Gal80* driver). As described, we found that the *Δ50/Δ*113 allele combination was viable [45]. Surprisingly, motor neuron-specific expression of the GFP-KH1* and KH1*KH2* transgenes caused embryonic lethality in *Δ50/Δ*113

mutant flies when raised at 25˚C. However, we observed escapers when raised at 20˚C. As a result, we were able to conduct all experiments below in a *Δ50/Δ*113 *(-/-)* loss-of-function background.

We next examined FMRP granules in 4-day old primary motor neuron cultures from dissociated larval ventral ganglia. All cells expressing WT-FMRP formed generally small, round granules in the soma (Fig 5A and 5B). Similarly, all cells expressing KH2* formed granules but, like what we observed in S2R+ cells, they were less numerous and sometimes formed amorphous structures (Fig 5A). Strikingly, granules formation was significantly reduced or eliminated in KH1* and KH1*KH2* mutants (2% and 0% respectively) suggesting that the KH1 domain is required to form FMRP granules in neurons (Fig 5A and 5B). The level of expression of each KH mutant was similar, indicating that this result was not likely due to reduced protein concentrations (Fig 5C). Both WT-FMRP and KH2* granules were also found in neurites (Fig 5D). However, there were significantly fewer GFP-KH2* granules outside of the soma (Fig 5D and 5E). Despite this, mutant granules were found in similar proportions in distal regions of neurites (Fig 5F). These data suggested that the KH2 domain may be required for FMRP granule transport. However, we cannot rule this being a stochastic effect of reduced granule formation.

KH2 domain is required for FMRP granule trafficking in neurites

We next asked if the KH mutations caused defects in the transport of FMRP granules. As GFP-KH1* and KH1*KH2* do not form any granules in neurites (Fig 5A), we focused on *KH2**,-/- compared to *WT-FMRP*,-/-. Consistent with recent findings of GFP-tagged FMRP in hippocampal neuron dendrites, the majority of neuritic WT-FMRP granules were stationary (Fig 5G) [10]. Interestingly, the proportion of mobile granules in KH2 mutants was higher in both anterograde and retrograde directions (Fig 5H). Moreover, the average velocity of KH2* granule transport in the anterograde direction was significantly increased (Fig 5J). Interestingly, we noted that some KH2* granules appeared to undergo bursts of rapid movement in the anterograde direction (Fig 5I; asterisk in kymographs). The was a phenotype we did not observe with WT-FMRP granules. Despite this increase in net velocity, total granule displacement was not significantly altered (Fig 5K). This finding is consistent with our observation that the percentage of KH2* granules in distal neurites is the same as WT-FMRP granules (Fig 5F). Collectively, our data suggests that the reason there fewer KH2* granules in neurites is likely due to a general defect in the formation of granules in the soma.

The KH2 domain regulates the dynamics of FMRP in neuronal granules

We next performed FRAP analysis in primary *Drosophila* motor neurons, looking at somatic and neuritic granules as two separate populations (Fig 6A–6D). In agreement with published results, the mobile fraction of WT-FMRP was significantly lower in both the soma and neurites (16% and 9% respectively) of cultured neurons than in S2R+ cells (82%) suggesting that a larger proportion of WT-FMRP in NGs is found within the non-dynamic, immobile fraction (Figs 6E and 3C) [35,46]. Moreover, the recovery time of WT-FMRP in the mobile pool was about 2-fold slower in neuritic granules ($t_{1/2}$ = 25s) than in those found in the soma ($t_{1/2}$ = 12s) (Fig 6E and 6F). Together, these data suggest that wild-type FMRP granules in neurons have distinctly different dynamic than those that form in S2R+ cells. There were two observations with KH2* granules that support the conclusion that this mutation alters FMRP granule dynamics in neurons. First, the amount of KH2* found in the mobile fraction was significantly greater in both somatic and neuritic NGs (27% and 27% respectively, Fig 6E). Second, the recovery time of KH2* in the mobile fraction was reduced ($t_{1/2}$ = 7s and 8s respectively;

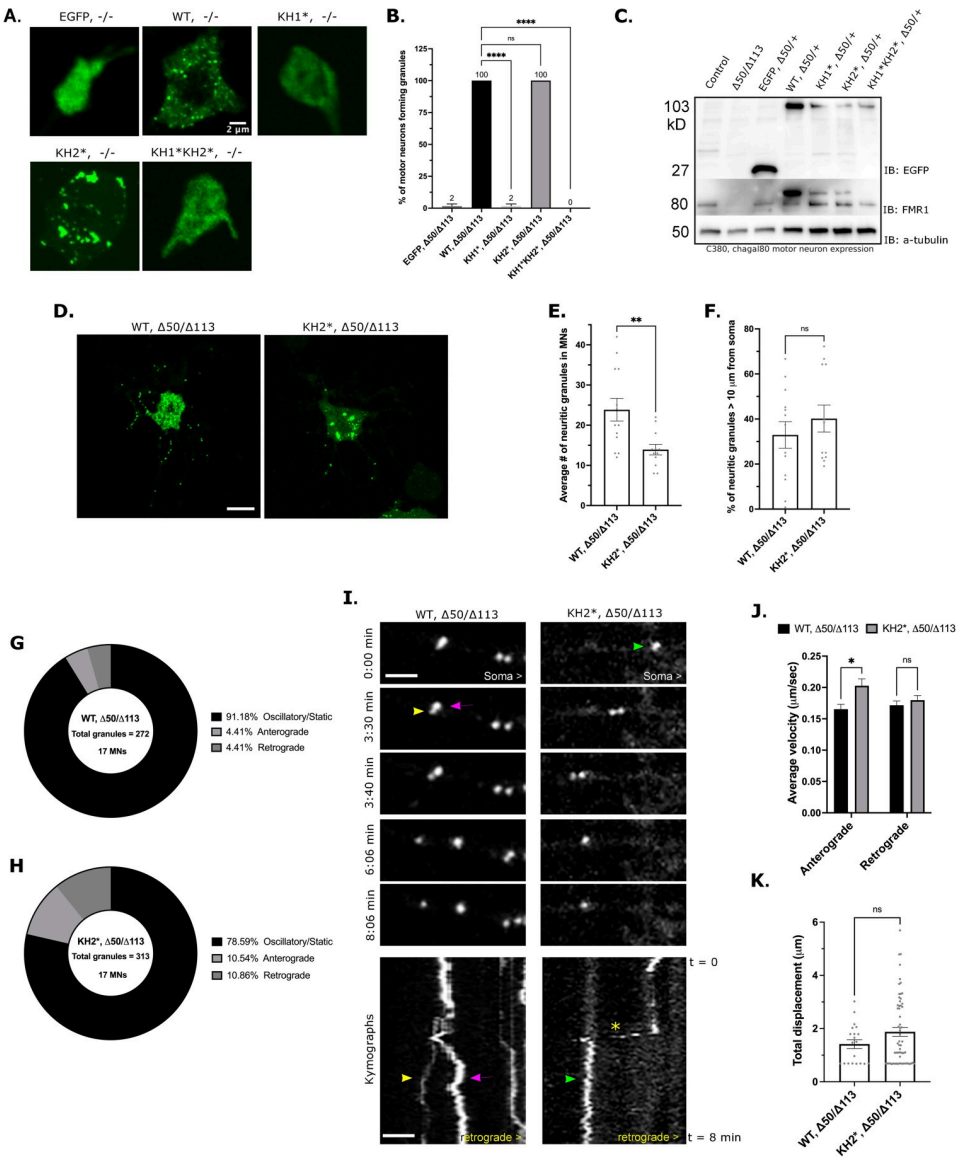

Fig 5. FXS-causing mutations disrupt NG formation and trafficking in neurons. (A) Representative images of major granule phenotype in primary neuron cell bodies. Expression of the indicated transgene was driven by *C380-Gal4*, *cha-gal80*. Scale bar = 2μm. (B) Percent of GFP-positive motor neurons forming FMRP granules in the *dFmr1* $^{-/-}$ null mutant background. Average is shown above respective bar (mean ± SE; 20 cells per triplicate, one-way ANOVA). (C) Western blot analysis of EGFP (top), FMRP (middle), and α-tubulin (bottom) expression under the *C380-Gal4*, *cha-gal80* selective motor neuron driver in the *dFmr1* $^{-/+}$ larval CNS to show expression of each transgene relative to 50% expression of endogenous FMRP (lower band). The upper band marks the EGFP-FMRP (and mutant) fusion proteins. (D) Representative images of *WT*, -/- and *KH2**, -/- primary MNs. Scale bar = 10μm. (E) Quantification of the average number of NGs within neurites of primary MNs (mean ± SE; 13 and 12 MNs, unpaired t test). (F) Percentage of neuritic granules in (E) that are ≥10 μm from the MN cell body (mean ± SE; 13 and 12 MNs, unpaired t test). Pie charts representing the fraction of neuritic granules that remain stationary (static/oscillatory) or move in the anterograde or retrograde direction (relative to the cell body) in *WT*, -/- (G) or *KH2**, -/- (H) primary neurons. Percentages are annotated in the legend for each chart (n = total granules in 17 MNs). (I) Time-lapse images and kymographs illustrating NG movements within neurites of WT (left panel) and KH2* (right panel) NGs. Images are oriented with the cell body on the right. Each granule is annotated with a colored arrowhead which corresponds with the traces in the kymograph. The asterisk marks a KH2 granule that exhibits a short burst of rapid movement. Scale bar = 2 μm. (J) Comparison of anterograde and retrograde velocities of motile WT-FMRP and KH2* NGs in neurites (mean ± SE; 56 and 61 granules / category; two-way ANOVA). (K) Average total displacement (μm) of all motile WT and KH2* NGs (mean ± SE; unpaired t test). In all graphs: * p<0.05, **p<0.01, ***p<0.001, ****p<0.0001.

https://doi.org/10.1371/journal.pgen.1010084.g005

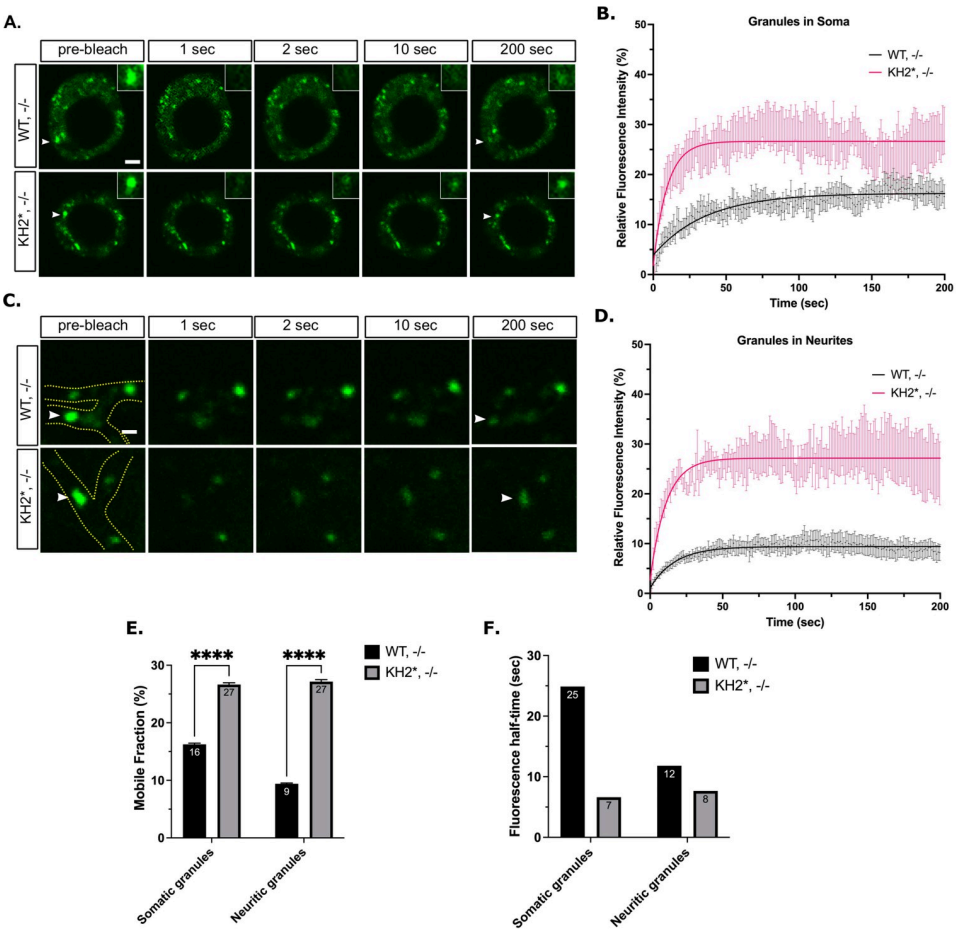

Fig 6. FXS-causing mutations in FMRP disrupt NG dynamics in neurons. (A) Representative FRAP time lapse images of somatic NGs pre- and post-bleaching event. Arrowheads point to the bleached granule. Scale bar = 2 μm. (B) Fluorescence recovery curves of somatic NGs over 200 seconds (mean ± SE; n = 13 granules WT and 12 KH2*). (C) Representative FRAP time-lapse images of neuritic NGs pre- and post-bleaching event. Neurites are outlined in green in the pre-bleach image, arrowheads point to the bleached granule. Scale bar = 1μm. (D) Fluorescence recovery curves of neuritic NGs showing fluorescence intensity relative to the initial pre-bleach intensity over 200 seconds (mean ± SE; n = 9 and 11 granules). (E) Quantification of the average mobile fractions of somatic (left) or neuritic (right) mobile fraction of WT and KH2* NGs (unpaired t test; $p < 0.0001$). (F) Quantification of the fluorescence half-time ($t_{1/2}$) of somatic and neuritic WT and KH2* NGs in seconds. Granules are those analyzed in B-E.

https://doi.org/10.1371/journal.pgen.1010084.g006

Fig 6F). These data further indicate that the composition and dynamics of FMRP granules have been significantly altered by the KH2 mutation and suggest that the KH2 domain is required to stabilize FMRP granules in neurons.

The KH1 domain is essential for the translational repression activity of FMRP

We next wanted to examine the role of the KH domains in regulating the translational repression activity of dFMRP. Both KH1* and KH2* have been shown to disrupt the association of mammalian FMRP with polysomes suggesting that the KH domains are important for translational repression [17,18,22,26]. Moreover, the KH domains of dFMRP bind directly to the 80S ribosome and can block elongation *in vitro* [47]. To further examine the role of the KH domains in translational control, we used a λN-based tethering assay in S2 cells, where the

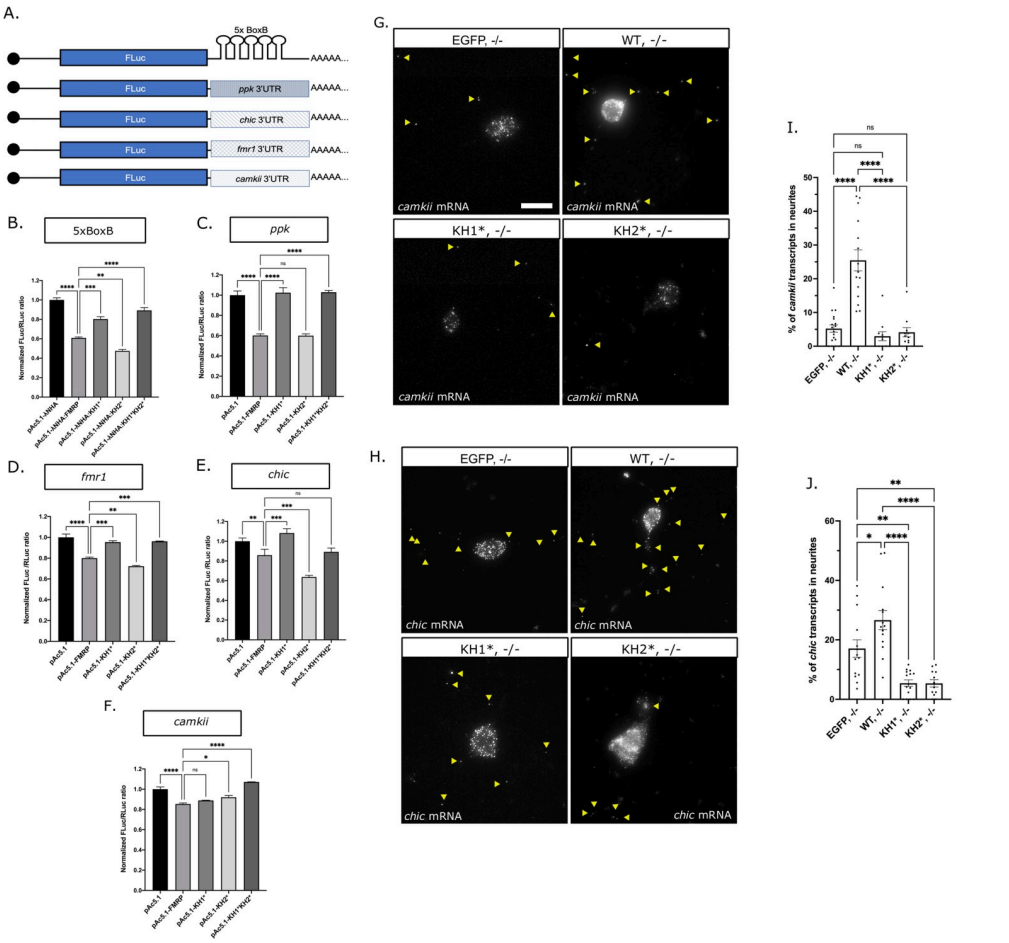

Fig 7. FXS-causing mutations disrupt translation and RNA transport. (A) Diagram of the FLuc reporters used in this study fused to the *SV40 3'UTR* containing the 5xBoxB sequence or to the 3'UTR's of known mRNA targets of dFMRP. Luciferase assays of (B) λN:HA-tethered FMRP-mutants repression of the 5xBoxB FLuc reporter or the untethered FMRP-mutants repression of FLuc fused to the (C) *pickpocket* (*ppk*), (D) *fmr1*, (E) *chickadee (chic)* or (F) *camkii* 3'UTR. FLuc/RLuc ratios were normalized to empty vector ratios. Graph shows repression of the FLuc reporter by empty vector or FXS-causing point mutants compared to *pAc5.1-λNHA:FMRP (B) or pAc5.1-FMRP (C-F)* (mean ± SE; one-way ANOVA). Representative images of *camkii* (G) or *chic* (H) mRNA smFISH in primary MNs. Yellow arrowheads in images are distinguishing transcripts found in neurites. Scale bars = 10μm. Quantification of the average number of *camkii* (I) or *chic* (J) transcripts in neurites of each of the FMRP mutants (mean ± SE of 11–18 MNs; unpaired t test). In all graphs: * p<0.05, **p<0.01, ***p<0.001, ****p<0.0001.

https://doi.org/10.1371/journal.pgen.1010084.g007

3'UTRs of known dFMRP target mRNAs were fused to the 3' end of a firefly luciferase reporter, or FLuc (Fig 7A). To eliminate RNA binding as a mechanism, we first tethered λN-tagged FMRP constructs directly to the reporter via a 5X tandem BoxB sequence that was inserted into the heterologous *SV40* 3'UTR. The WT-FMRP and KH2* constructs were both able to repress translation (Fig 7B). In contrast, the ability of KH1* to repress reporter expression was significantly disrupted, suggesting that the KH1 domain is required for repression activity.

Next, we determined whether untethered dFMRP could repress the translation of Fluc by binding to the 3'UTRs of known targets mRNAs and if either of the KH domains were required for this to occur. We replaced the *SV40* 3'UTR containing the BoxB repeats with the 3'UTRs from mRNAs encoding for: 1) the degenerin/epithelial sodium channel (DEG/ENaC) family member, *pickpocket* (*ppk*); 2) the Ca^{2+}/calmodulin-dependent protein kinase II, *camkii*;

3) the profilin ortholog, *chickadee (chic)*; and 4) its own mRNA, *fmr1* [33,48–50] (Fig 7A). As with the BoxB reporter, the KH1 domain was required to regulate repression of the *ppk*, *chic*, and *fmr1* reporters as repression was ameliorated in KH1* and KH1*KH2* (Fig 7B–7E). The efficiency of repression of each of these reporters by WT-FMRP and KH2* was variable, likely due to differences in the ability of these proteins to interact with or bind to the 3'UTR. In contrast, the *camkii* reporter was different in that repression is only slightly derepressed by KH2* and KH1*KH2* (Fig 7F). Collectively, these data indicate that FXS-causing mutations in the KH1 and KH2 domains can differentially regulate translational repression. The derepression of translation in KH1* correlates with defects in its ability to form FMRP granules in cells and neurons (Figs 2 and 5).

The KH domains are required for the transport of FMRP target RNAs

NGs are specialized MLOs within neurons that serve to transport translationally silent mRNAs between the soma and axonal or dendritic compartments [51]. Therefore, we next asked if *KH1*,-/- or *KH2*, -/- neurons had defects in mRNA localization. To address this, we used single-molecule fluorescence *in situ* hybridization (smFISH) to quantify transcripts in the soma and neurites. We focused on two mRNA targets of dFMRP in flies, *chic* and *camkii*, both of which have been shown to interact with dFMRP-containing NGs in primary motor neurons [30,46]. Their translational repression is also regulated by the KH1 and KH2 domains (Fig 7E and 7F). We find that there are significantly more *camkii* and *chic* transcripts in *WT-FMRP*,-/- neurites compared to controls suggesting that dFMRP promotes the transport of both mRNAs to neurites (Fig 7G–7J). The percentage of both *chic* and *camkii* transcripts found in neurites is significantly reduced in KH1* and KH2*. Because some transcripts still localize, these data suggest that the *chic* and *camkii* mRNAs can localize to neurites through a KH domain-dependent and independent mechanism.

Discussion

FMRP has been implicated in a growing number of biological processes in neurons ranging from the control of translation and RNA transport to the regulation of RNA editing, splicing, genome stability, and ion channel function [52]. Because the vast majority of FXS cases are caused by loss of FMRP expression, it has been difficult to determine which of these functions are involved in FXS pathophysiology. In contrast, the study of disease-causing missense mutations in FMRP has allowed for the isolation of specific protein functions that may be contributing to FXS phenotypes [15]. Here, we provide multiple lines of evidence that FXS-causing mutations in the KH domains differentially affect FMRP granule assembly, dynamics, and function in *Drosophila* neurons. First, an FXS-causing missense mutation in the KH1 domain disrupts the ability of FMRP to form granules in primary neuron cell culture (Fig 5A and 5B). In contrast, KH2 mutants form granules in the soma but their localization to distal neurites is reduced (Fig 5D–5F). Second, we find that KH2* significantly decreases the amount and stability of FMRP found in the mobile fraction of neuronal FMRP granules (Fig 6E and 6F). Third, the KH domains are differentially required to regulate the translation of reporters for known target mRNAs (Fig 7B–7F). Finally, both KH domains are required to promote the localization of specific target mRNAs to neurites (Fig 7G–7J). Translational repression and RNA transport are processes that have been directly attributed to FMRP-containing RNA granules in neurons [3].

Based on these data, we propose the following model describing the role of the KH domains in FMRP granule formation in neurons (Fig 8A). Specificity is conferred by interactions between the C-terminal RGG domain of FMRP and structured sequences in target RNAs. The

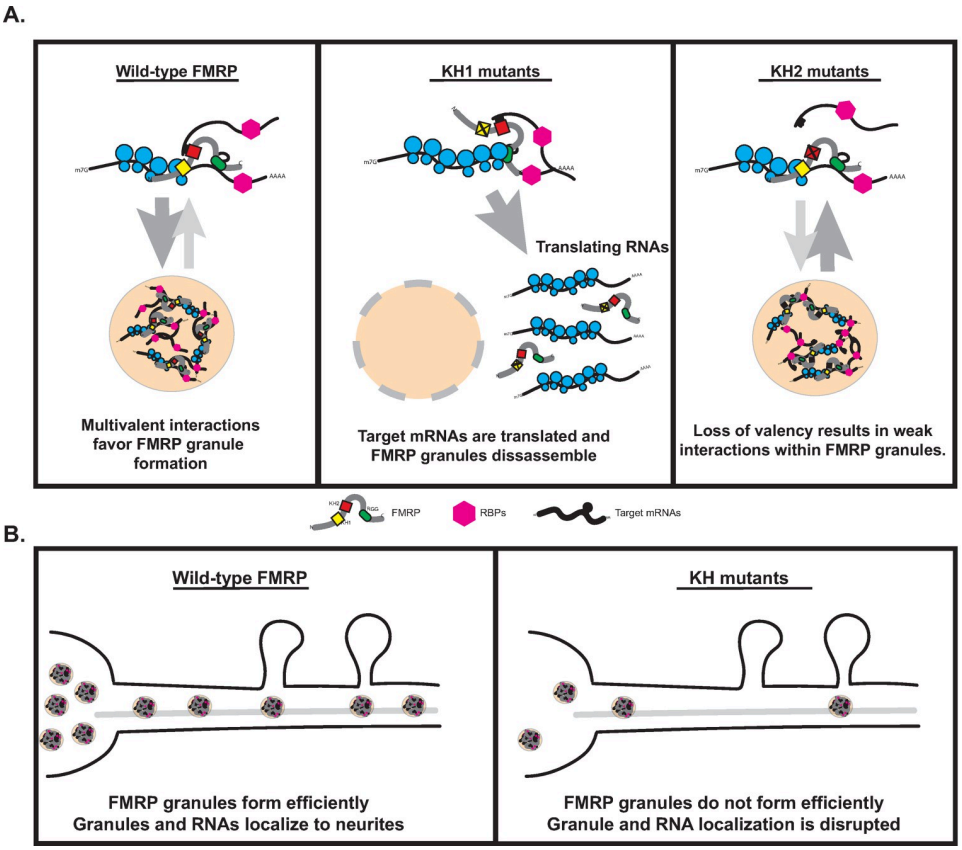

Fig 8. Model for FMRP granule assembly and the contribution of the KH domains. (A) The proposed mechanism by which the KH1 and KH2 domains regulate FMRP granule formation in *Drosophila* neurons. The KH1 domain interacts with ribosomes to block translational elongations, a process linked to the formation of FMRP granules in mammalian neurons [10]. Disruption of the KH1 domain results in the targeting of bound target mRNAs to the translating pool outside of granules and disrupts granule formation. The KH2 domain interacts with unknown mRNAs via weak, promiscuous interactions strengthening associations within granules. Disruption of KH2 weakens these interactions, destabilizing FMRP granules, and disrupting their formation. (B) The proposed mechanism by which disruption of the KH domains impact mRNA localization. Either failure to form granules (in KH1 mutants) or decreased formation (KH2 mutants) results in fewer granules available to deliver mRNA cargos in neurites.

https://doi.org/10.1371/journal.pgen.1010084.g008

KH1 domain interacts directly with stalled polyribosomes, a process that has been linked to FMRP granule formation in mammalian neurons [10]. In KH1* mutants, transcripts re-enter the translating pool leading to granule dissociation. In contrast, the KH2 domain interacts weakly and nonspecifically with RNAs in granules providing increased valency and helping to regulate FMRP granule integrity. FMRP can still bind specifically to targets and the KH1 domain can still interact will polysomes. In KH2* mutants, granules are destabilized because the fail to interact non-specifically with other RNAs found in granules. In both cases, the inhibition of FMRP granule formation disrupts localization of target mRNAs to neurites (Fig 8B).

Several results in S2 cells contradict data from primary neurons. One notable difference was that KH1* and KH1*KH2* were both capable of forming granules in S2 cells (at reduced levels) but not in primary neurons (Figs 2C, 2D, 5A and 5B). There are several possible explanations for this observation. First, FMRP constructs are expressed in S2 cells using the strong promotor from the fly *actin 5C* gene. Thus, concentrations of FMRP within transfected cells may be high enough to overcome concentration thresholds needed to drive granule formation. Second, our experiments in S2 cells were done in the presence of endogenous FMRP. Some

evidence suggests that mammalian FMRP may form a dimer through N-terminal Agenet domains [53]. Therefore, it is possible that some of the KH1* and KH1*KH2* protein is being recruited to granules containing endogenous FMRP in S2 cells by protein-protein interactions. Finally, the assemblage of RNAs present in S2 cells and neurons is likely to be distinctly different. It is likely that these RNAs are differentially influencing granule formation.

The disordered C-terminus of mammalian FMRP is necessary and sufficient to drive the formation of phase-separated droplets *in vitro* [14]. Furthermore, phosphorylation patterns of amino acids in this region control the propensity to phase separate in the presence of RNA and to regulate rates of deadenylation and translation within these condensates [54]. Collectively, these data suggest that regulation of FMRP phase separation might be a simple mechanism to allow for the delivery of translationally repressed mRNAs to synapses and to control their local translation in response to activity. Through our analysis of *Drosophila* FMRP granules in cells, we show that the C-terminal IDR is sufficient to regulate granule formation (Fig 1D). However, granule formation is significantly enhanced by the addition of the structured KH domains (Fig 1D). This is consistent with current models suggesting that MLO formation *in vivo* is driven by multivalent interactions between protein and RNA components [12,13]. Increased valency provides a scaffold of *cis*-acting binding sites that allow for interactions with multiple *trans*-acting partners, allowing interacting molecules to compartmentalize within the cell [55,56]. Published findings also show that different types of NGs are generally more stable than other types of MLOs [31,51,57–59]. In support of this, we find that WT-FMRP granules are significantly less dynamic in primary neurons than in S2R+ cells (Figs 3 and 7). This stability is likely to be necessary so that FMRP granules can resist the shear stress associated with active transport.

While the precise RNA binding sites are a source of debate, the KH domains clearly bind with different specificity and/or affinity to target mRNAs [60]. The KH1* and KH2* mutations are predicted to disrupt the proper folding of each RBD and to disrupt functions of FMRP including mRNA-binding [22,26,36]. Analysis of this KH2* (I307N) and a different KH1 mutant (I244N) in *Drosophila* FMRP suggest that neither mutation causes an overall change in the structure of the mutant proteins [47]. The KH1*KH2* or ΔKH mutants have been examined. Therefore, the simplest explanation for the role of the KH2 domain in regulating FMRP granule formation and dynamics is that it is working with other interacting domains (RGG box, IDR, etc.) to increase valency through weak interactions with RNA. Why does the KH1 mutation have a more significant impact on FMRP granules? It is possible that the KH1 domain is contributing disproportionately strong (or numerous) interactions with mRNAs which is shifting the critical concentration needed for granule formation. Interactions occurring via KH1 could be shifting the concentration threshold required to promote FMRP granule formation. For example, multivalent interactions between RNA and proteins such as hnRNPA1 and FUS, influence LLPS by shifting the phase boundary and requiring lower protein concentrations to initiate demixing [14,61,62]. Alternatively, KH1 may regulate FMRP granule formation by interacting with stalled polyribosomes.

Our analysis of KH domain function reveals a link between FMRP granule formation and translational repression in neurons. A significant fraction of mammalian and *Drosophila* FMRP interacts with polysomes and this association is disrupted by the G266E and I304N mutations [17,18,26,63]. One mechanism by which FMRP blocks translation is by interacting with stalled polysomes [64]. More specifically, the KH domains of dFMRP interact directly with the peptidyl site of ribosomes [47]. This suggests a mechanism by which FMRP stalls translational elongation by sterically inhibiting tRNA entry. The non-disease associated KH1 mutant (I244N) and KH2* (I307N) both disrupt binding affinity, with the I244N mutation having a stronger effect [47]. Interestingly, analysis of FMRP granules in mouse brain

homogenates by electron microscopy found that FMRP and ribosomes both localize to a subset of neuronal RNA transport granules [10]. These data led the authors to propose that FMRP granules form from stalled polysomes. A prediction from this model is that disruption of FMRP-ribosome association would negatively impact the formation of a subset of FMRP granules. Our data provide support for this model as we show that KH1* and KH2* both disrupt FMRP granules, with the KH1 mutant having a stronger effect (Figs 2C, 2D, 5A and 5B). We also demonstrate that the KH1 domain is required to repress the translation of most translational reporters tested, including when FMRP was directly tethered to a heterologous 3'UTR (Fig 7B–7E). Additional studies would be required to determine if there is a direct connection between polysomes, ribosome stalling, and FMRP granule formation in *Drosophila* neurons. This would also help to clarify whether FMRP granules are a cause or consequence of translational repression.

In cultured mouse neurons, the specificity of FMRP for mRNAs targeted for transport to neurites is conferred by interactions between its C-terminal RGG domain and G-quadraplex sequences within the 3'UTRs of localized mRNAs [65]. This study also found that the FXS-causing KH2 mutant (I304N) which disrupts ribosome association retained the ability to promote the localization of G-quadraplex-containing transcripts to neurites. In contrast, we show that both the KH1 and KH2 mutants fail to promote the localization of *chic* and *camkii* to neurites in cultured *Drosophila* neurons (Fig 7G–7J). The long *chic* 3'UTR (but not *camkii*) contains G-rich sequences predicted to fold into quadraplexes suggesting that localization of these fly mRNAs may be regulated by a G-quadraplex-independent mechanism. This might be due to our limited sample size as mouse studies focused on a global analysis of mRNA localization [65]. Alternatively, the control of mRNA transport by *Drosophila* FMRP may be mechanistically different. The RGG domain found in dFMRP is not highly conserved and it fails to bind with high affinity to the *sc1* RNA, a G-quadraplex-containing target for human FMRP [66]. Unlike in mouse studies, we also observe both transcript- and KH domain-specific coupling of translational repression and mRNA localization in *Drosophila* neurons (Fig 7) [66]. It is possible that this represents a *bona fide* difference between fly and mammalian FMRP.

The role of FMRP granules in the transport and translation of target mRNAs in neurons is complex because their organization, dynamics, and function are regulated by multivalent interactions involving both structured and unstructured protein domains. Our data support a model where FMRP granules are metastable, solid-like, MLOs. This is a state that is likely necessary to allow for their active transport in neurites without the loss of RNA and protein components. We demonstrate that the KH1 and KH2 domains are required to maintain FMRP granule integrity in both S2R+ cells and neurons. FXS-causing mutations disrupt this equilibrium, leading to the formation of MLOs that are unstable. This is distinctly different from disease-causing mutations in IDR-containing RBPs that have been linked to neurodegenerative disease such as TDP-43, FUS, or hnRNP-A1, which lead to the formation of metastable, then stable, pathological inclusions [61,67]. That said, our studies have revealed novel granule phenotypes associated with FXS-causing KH mutations. First, both KH mutations disrupt the sensitivity of SGs to 1,6-HD, suggesting that their biophysical properties have been altered (Fig 4D–4H). KH1* has a more significant impact on this phenotype than KH2*. Second, MN-specific genetic "rescue" experiments with KH1* causes lethality in an otherwise viable *dFmr1* loss-of-function background suggesting that G266E may be an uncharacterized gain-of-function mutation. Finally, the KH1 mutation also nearly abolishes FMRP granule formation in neurons. These results may explain why the G226E mutation causes such a severe form of FXS [26].

Methods

Fly stocks and husbandry

In all experiments, both male and female flies were used. Most crosses were incubated at 25˚C with 12-hour light/dark cycles and 60% humidity on standard Bloomington medium. For primary motor neuron cell culture, crosses were raised at 20˚C through the third instar stage to bypass larval lethality seen with KH1* and KH1*KH2* at 25˚C. Fly lines used and made in this study are listed in S1 Table. Plasmid constructs for the generation of transgenic lines were constructed as described below. All transgenes were injected into fly strain 24485 for *PhiC31*-mediated integration into the same site on chromosome III. All transgenes were recombined with the $dFmr1^{\Delta 50M}$ null allele.

Cell culture

S2 and S2R+ cells were maintained at 24˚C with ambient humidity in a dark incubator in M3 +BPYE media. S2-DRSC cells were used for luciferase reporter assay experiments. S2R+ cells were used for imaging experiments due to their higher propensity to adhere to and flatten out on poly-D-lysine coated cover slips. Cells and media recipes were obtained from the *Drosophila* Genomics Resource Center (DGRC). Primary motor neurons were cultured from wandering 3rd instar larvae using a protocol adapted from Barbee et al. 2006. For each genotype, ventral ganglia from ten third instar larvae were dissected, dissociated, and then grown in complete M3+BPYE media (M3+BPYE supplemented with 50 μg/mL insulin) for 3 to 5 days prior to imaging.

Cloning and site directed mutagenesis

The backbone vector for all S2 cell culture plasmids is a modification of pAc5.1 (ThermoFisher Scientific, Waltham, MA) which drives expression from the fly actin 5C gene. For imaging of FMRP, the coding region of the *FMR1-RD* cDNA (LD09557; DGRC) was PCR amplified and cloned downstream of EGFP in the pAc5.1B-EGFP vector (a gift from Elisa Izaurralde; Addgene plasmid #21181) using the *HindIII* and *EcoRI* restriction sites to make pAc-B5.1-EGFP-FMRP. The pAc5.1:EGFP-FMRP-IDR, pAc5.1:EGFP-FMRP-ΔIDR, pAc5.1:EGFP-FMRP-KH:IDR and pAc5.1:EGFP-FMRP-ΔKH plasmids were all constructed by PCR amplification of the indicated sequence followed by cloning into pAc5.1B-EGFP. Primer sequences and restriction sites are listed and described in S2 Table. The *Drosophila* G269E and I307N mutations were generated using the Q5 Site-Directed Mutagenesis Kit (New England Biolabs, Ipswitch, MA). Mutagenesis primers were designed using the "substitution" feature in NEBaseChanger v1.2.9 (New England Biolabs). Mutagenesis occurs at nucleotide 805–807 (GGA→ GAA) and nucleotide 868–870 (ATC→ AAC) in the KH1 and KH2 domain, respectively. Each mutation was introduced directly into the pAc5.1B:EGFP-FMRP vector. The KH1*KH2* double mutant was created by introducing both mutations sequentially (KH1* followed by KH2*).

Plasmids for the generation of transgenic fly lines were all constructed as follows. The EGFP-FMRP sequence for WT-FMRP and each mutant construct were PCR amplified from their respective pAc5.1 vector using primer sequences listed and described in S2 Table. Products were then cloned directionally into the 5'-*KpnI* and 3'-*XbaI* sites of pUAST-attB. Transgenic flies were generated as described above.

To construct the pAc5.1-Rin-mCherry plasmid, we first generated a pAc5.1B-MCS-$(Gly_4Ser)_3$-mCherry plasmid. The Rin cDNA was obtained by reverse-transcriptase PCR from RNA extracted from wild-type (*CantonS*) adult flies. Total RNA was extracted using the Direct-zol

RNA kit (Zymo Research, Irivne, CA) and cDNA was generated using the RNA to cDNA Eco-Dry Premix Oligo dT kit (Takara Bio USA, Moutain View, CA). Rin was PCR amplified using primers listed and described in S2 Table and cloned into the *HindIII* and *EcoRI* restriction sites of pAc5.1-MCS-$(Gly_4Ser)_3$-mCherry to generate the final pAc5.1:Rin-$(Gly_4Ser)_3$-mCherry vector.

To construct plasmids for the tethered FLuc reporter assays, the wild-type dFMR1 and KH1*, KH2*, or KH1*KH2* mutants were PCR amplified from their respective pAc5.1-B-EGFP vector and cloned into the *HindIII* and *EcoRI* sites of the pAc5.1-lambdaN-HA vector (a gift from Elisa Izaurralde; Addgene plasmid #21302) [68]. For the untethered reporter assays, the indicated dFMR1 constructs were cloned into the MCS of pAc5.1B lacking the lambdaN-HA tag. The BoxB reporter was pAc5.1C-Fluc-Stop-5BoxB (a gift from Elisa Izaurralde; Addgene plasmid #21301) [68]. To construct the *camkii* and *Fmr1* reporters, the *SV40* 3'UTR and the 5xBoxB sequence was removed by digesting pAc5.1C-Fluc-Stop-5BoxB with *EcoRI* and *XhoI*. The long 3'UTR isoform of *camkii* and *Fmr1* were amplified by RT-PCR (as described for Rin) using primers listed and described in S2 Table. The 3'UTRs were then cloned into the cut plasmid via Gibson Assembly using the Gibson Assembly Master Mix (New England Biolabs). The 3'UTRs of *ppk* and *chic* were amplified by RT-PCR, cloned into pENTR D-TOPO, and into the pAc5.1-FLuc2 [dPolyA] RfA destination vector as we have previously described [69].

S2 cell transfections

DNA transfections were performed with the Effectene Transfection Reagent kit (Qiagen). Transient transfections were performed following the manufacturer's protocols. For fluorescence experiments, DNA constructs were transfected into S2R+ cells in 12-well plates. Cells were transfected with 0.5 μg of each construct except for pAc5.1B-EGFP:FMRP:KH1* in which 0.75 μg of DNA was used. Transfected cells were grown for ~ 72 hours before imaging. For luciferase assays, S2-DRSC cells in 24-well plates were transfected with 0.025 μg of the FLuc reporter plasmid, 0.1 μg of the *Renilla* luciferase (RLuc) transfection control plasmid, and 0.25 μg of either the pAc5.1/pAc5.1-λN control vector or the pAc5.1:FMRP/pAc5.1-λN:FMRP wild-type or mutant constructs. Transfected cells were grown for ~ 72 hours prior to analysis in luciferase experiments.

S2 cell imaging and granule analysis

S2R+ cells were transferred to poly-D lysine coated #1.5 cover glass bottom dishes (Cellvis, Mountain View, CA) within two hours of imaging. In all experiments, images were obtained using an Olympus FV3000 scanning confocal microscope with a 100x (NA 1.4) objective digitally zoomed to 2.95x (the optimal setting per the Fluoview software). To quantify the number of granules formed by each construct, 15 cells were analyzed in a single experiment. The single z-plane where the nucleus took up the largest cell area was imaged. Punctate areas of fluorescence intensity above background (at least 3 x 3 pixels which is 0.252 x 0.252 μm in these images) were classified as granules and were quantified using the Cell Counter plugin in ImageJ2/FIJI. For each image, cell diameter (through the longest axis in the same z-plane) and granule number were collected. From this, the number of granules per cell area (μm^2) was recorded. To count the number of transfected cells able to form granules, ~ 100 cells per FMRP construct were manually identified at the microscope. The total number of cells that formed granules out of all EGFP-expressing cells were quantified. Cells were scanned in z to make sure that granules in all planes were identified. The number of cells that formed granules was divided by total number of transfected cells for three separate experiments. To quantify

granule size, images were manually thresholded to include as many granules as possible without overlap. Size was determined using the Analyze Particles plugin in ImageJ2/FIJI. To compare the propensity of the different mutants to form circular granules, ~ 100 granule forming transfected cells were identified at the microscope. The number of cells forming circular and amorphic (non-circular) granules were counted. In most cases, cells that formed amorphous granules also contained circular granules, however, cells that formed any number of amorphous granules were categorized as amorphic.

Fluorescence recovery after photobleaching (FRAP) experiments

For all FRAP experiments, 17–21 EGFP positive granules were imaged using an Olympus FV3000 scanning confocal microscope with a 100x (NA 1.4) objective digitally zoomed to 2.95x (optimal settings). Granules selected for FRAP analysis generally fit into the "spherical" category. Granules selected for analysis in primary neurons were clearly in the cell body or neuritic compartments. In all cases, granules were photobleached with the lowest laser intensity necessary to completely bleach the granule, ranging from 2.44–10% 488nm laser power for 500–1,000 milliseconds. Two pre-FRAP images were collected and images were captured every 1.0878 seconds pre and post bleaching for a total of 200 frames (~ 218 s). For image analysis, images were initially processed in ImageJ2/FIJI) and analyzed essentially as described [70]. A ROI was manually traced in each FRAP movie for 1) the bleached granule, 2) an unbleached granule and 3) diffuse cytoplasmic staining for background. As necessary, the ROI was moved if/when granules moved in x/y out of the initially set ROI. If a granule clearly dropped out of the focal plane, it was excluded from analysis. The mean fluorescent intensity was obtained for each frame. The following was calculated: 1) Photobleach Correction Value (PCV), in which the average intensity of the pre-bleach unbleached granule was divided by the value for each subsequent unbleached granule, 2) Corrected Average Intensity (CAI), where the bleached granules mean intensity was multiplied by the PCV, 3) Background Corrected Fluorescence Intensity (BCFI), where the CAI was subtracted by the average intensity of the background ROI, and 4) the Final Corrected Value (FCV) which was calculated by dividing each BCFI by the initial BCFI value and multiplying by 100 to get a normalized fluorescence intensity profile. The FCVs from each movie were then analyzed a one-phase association, nonlinear fit in Graphpad Prism to calculate the fluorescence recovery curve, mobile fraction, and half-life.

Immunocytochemistry

S2R+ cells were transferred to poly-D lysine coated #1.0 cover glass bottom dishes (Cellvis) and allowed to settle for ~ 20 minutes. Cells were then fixed with 4% PFA for 10 minutes followed by a 5-minute incubation in ice cold methanol. Cells were washed three times for 5 minutes in PBS, permeabilized in PBST for 10 minutes, and then blocked in PBST with 2% BSA and 5% normal goat serum for 30 minutes. Cells were then incubated with primary antibodies overnight at 4˚C, washed three times for 5 minutes in PBS, and then incubated for 1 hour in secondary antibodies at room temperature. Finally, cells were washed with PBS and then mounted in DAPI-Fluoromount-G Clear Mounting Media (ThermoFisher Scientific). EGFP: FMRP constructs were visualized by GFP fluorescence. For HPat, rabbit anti-HPat (1:1,500) [42] primary and goat anti-rabbit Alexa-567 (1:500) secondary antibodies were used.

Arsenite and 1,6-hexanediol treatment

For SG experiments, cells were co-transfected with the indicated pAc5.1B:EGFP-FMRP construct and pAc5.1-Rin-mCherry. About 72 h post transfection, cells were treated with 0.5mM

sodium arsenite in M3+BPYE media for 45 minutes to induce SG formation. Non-stressed cells went through the same procedure but were incubated in media that did not contain sodium arsenite. For colocalization analysis, cells were immediately fixed in 4% PFA for 10 minutes, incubated with ice cold methanol for 5 minutes and then washed 3 times for 5 minutes in PBS. Preparations were then mounted on coverslips as described above. FMRP and Rin were visualized by imaging GFP and mCherry fluorescence respectively. For the analysis of granules with treated with 1,6-HD, cells were co-transfected with pAc5.1:EGFP-FMRP constructs and pAc5.1-Rin-mCherry. Cells were subjected to arsenite stress (or not stressed) as described above. Following the 45-minute incubation (+/- sodium arsenite), cells were treated with M3+BPYE media (+/- sodium arsenite) containing 10% 1,6-HD. Approximately 100 live transfected cells were analyzed for the presence or absence of FMRP or Rin granules, in triplicate.

Colocalization analysis

To determine the degree to which FMRP mutants colocalized with SGs or PBs, 12–13 images were analyzed in ImageJ2/FIJI using the JACoP plugin [71]. Images were cropped to the smallest area possible to eliminate colocalization outside of the cell of interest and images for FMRP/HPat were background subtracted to a rolling ball radius of 50 pixels to account for the higher degree of HPat background staining. In JACoP, Pearson's coefficient results were recorded for analysis.

Western blotting

For the detection of EGFP-FMRP construct levels in S2R+ cells, transfected cells were harvested at three days post-transection from a 6-well plate. Cells were scraped and resuspended by pipetting up and down and 1.5 mL of cells were spun down at 1,000x G for 5 minutes at 4˚C. Cells were then resuspended in 400 μL of 2x Laemmli sample buffer + **β**-mercaptoethanol on ice. For westerns conducted on *C380*, *cha-Gal80/+; UAS:EGFP-FMRP*, $FMR1^{\Delta 50M}$/+ larvae ectopically expressing the wild-type and FXS-causing point mutants, 5 ventral ganglia (including optic lobes) were dissected and added to 100μL of 2x Laemmli sample buffer + **β**-mercaptoethanol on ice. Then, the ventral ganglia were homogenized in a 1.6 mL microcentrifuge tube for 30 seconds on ice using a hand-held homogenizer. Homogenates were incubated on ice for 3 minutes, and then processed as indicated above for S2R+ cells. For both assays, the primary antibodies used were mouse anti-dFMR1 (1:3,000; 6A15; Abcam, Cambridge, UK), rabbit anti-EGFP (1:2,000; Proteintech Group, Rosemont, IL), and mouse anti-α-tubulin (1:1,000; 12G10; Developmental Studies Hybridoma Bank, Iowa City, IA). Secondary antibodies used were horse anti-mouse HRP or goat anti-rabbit HRP which were both diluted 1:1,000 in block (Cell Signaling Technology, Danvers, MA). Blots were probed, stripped, and re-probed with the indicated antibodies to make direct comparisons within experiments.

Primary motor neuron imaging and neurite transport analysis

For analysis of *C380*, *cha-Gal80/+; UAS:EGFP-FMRP*, -/- larvae expressing either wild-type FMRP or the KH2 mutant, primary larval motor neurons were collected and cultured as described above. At 4 days post-harvest, live neurons were imaged using an Olympus FV3000 scanning confocal microscope with a 100x (NA 1.4) objective. For soma imaging, images were digitally zoomed to 2.95x for optimal resolution and a z-stack was obtained with 0.39μm slices through the entire soma. Images were presented as Z-projections made using ImageJ2/FIJI. For neurite transport analysis, live cells were imaged with a 100x objective (NA 1.4) digitally

zoomed to 1.79x so branching neurites could be imaged. Movies were collected containing four 0.39μm z-slices, over 100 frames (8:04 minutes). Movies were then analyzed using the Kymolyzer plugin in ImageJ2/FIJI from which granule velocities and directionality were obtained, using a lower speed limit set to the pixel size (0.138μm/s) [72]. A particular granule was stationary if its average velocity (in either direction) was below this minimum speed limit for the duration of the movie. Motile granules were classified as retrograde or anterograde based on net displacement towards or away from the cell body. Kymographs were generated using the KymographBuilider plugin in ImageJ/FIJI. To calculate the average number of neuritic granules in primary motor neurons, the max-intensity Z-projection of the first time point was used (Frame 1). The number of granules in the soma and neurites were manually counted using the Cell Counter plugin for ImageJ2/FIJI. Additionally, the proportion of neuritic granules 10μm or further from the cell body was determined from these images. The scale was globally set, and a symmetrical circle was drawn tightly around each cell using the oval selection tool in ImageJ, containing as much of the cell as possible. The diameter of each cell body was recorded in μm. The center of each circle was determined and marked using the Pencil tool. A line was drawn to the center of each granule within neurites and distance from the cell body was recorded in μm. These were subtracted by the radius for their respective cell body to obtain the final distance.

Luciferase reporter assays

Luciferase reporter assays were done essentially as we have described [69]. At three days post transfection, 75 μL of resuspended cells were added in three technical replicates to a 96-well white, flat bottom polystyrene assay plate (Costar, Washington, DC). FLuc and RLuc expression was measured using the Dual-Glo Luciferase Assay System kit (Promega, Madison, WI) per the manufacturer's instructions and luminescence detected using a Synergy HTX Multi-Mode Microplate Reader (BioTek, Winooski, VT). FLuc values were normalized to corresponding RLuc values. The FLuc/RLuc ratio for each experiment was normalized to its respective control. The experiment was repeated three times for each FLuc reporter.

Single molecule FISH and FISH-quant image analysis

For analysis of *C380*, *cha-Gal80/+; UAS:EGFP-FMRP*, -/- larvae expressing either wild-type FMRP or the KH2 mutant, primary larval motor neurons were collected and cultured as described above. Custom Stellaris FISH Probes were designed against *Drosophila melanogaster camkii* and *chic* by utilizing the Stellaris FISH Probe Designer (S3 Table; Biosearch Technologies, Hoddesdon, UK). Primary motor neurons were hybridized with the indicated Stellaris FISH Probe set labeled with either Quasar-570 or 670 (Biosearch Technologies) following the manufacturer's instructions. Briefly, at 3–4 days post culturing, cells growing on #1.5 cover glass were washed in PBS. Cells were then incubated in fixation buffer (3.7% formaldehyde in PBS) for 10 minutes at room temperature, then washed twice in PBS. To permeabilize cells were immersed in 70% ethanol at 4˚C for at least 1 hour and up to a week. Ethanol was aspirated and cells were washed in Stellaris Wash Buffer A for 5 minutes, then hybridized with the indicated probe(s) in a dark, humid hybridization chamber at 37˚C for 5–16 hours. Probes were used at a final molarity of 0.125μM in Stellaris Hybridization buffer. Hybridization buffer was aspirated, and cells were incubated with Wash Buffer A twice at 37˚C for 30 minutes, then washed with Stellaris Wash Buffer B for 5 minutes at room temperature. Buffer was aspirated and Vectashield Mounting Medium was added to the #1.5 cover glass in the imaging dish and a clean coverslip was placed on top and sealed with clear nail polish. Imaging dishes were stored in the dark at -20˚C for up to 2 days before imaging on an ONI Nanoimager S.

Approximately 15 cells were imaged per genotype using the widefield microscopy application. To detect smFISH probes, cells were exposed to 7% 570- or 640-laser power for 1,500 milliseconds. Z-projection was obtained with 0.2 μm slices through the entire cell. EGFP-FMRP was imaged sequentially which allowed us to distinguish the soma and neurites from background. To analyze smFISH images, we used the FISH-Quant Matlab application to detect, localize and quantify mRNA in primary motor neurons [73]. Motor neuron soma and neurites were outlined individually by hand, which allowed us to differentiate mRNAs residing within the soma and neurites.

Quantification and statistical analysis

All data were initially recorded in Excel (Microsoft) and then graphed and analyzed in Prism version 9.0.2 (GraphPad). Results were considered statistically significant if $p<0.05$. Error bars throughout the study indicate mean ± SEM. n.s. = not significant, * $p<0.05$, ** $p<0.01$, *** $p<0.001$, and **** $p<0.0001$. Outliers were identified and removed using ROUT method in Prism. Statistical tests and sample sizes for each experiment are indicated within the corresponding figure legend and/or in methods section.

Supporting information

S1 Text. Supplemental methods.
(DOCX)

S1 Fig. KH domain mutants disrupt FMRP function when overexpressed in larval MNs. (A) Wandering third instar larval NMJs from *C380-Gal4* (Control), *UAS-FMR1*, and *UAS-EGFP:FMRP* mutants were stained with antibodies targeting the postsynaptic density marker, DLG (green) and the neuronal membrane marker, HRP (magenta). Maximum Z-projections of NMJs in abdominal segment 3 innervating body wall muscles 6/7 were analyzed. Scale bar = 50μm. (B) Percentage of type 1b bouton number normalized to the area of muscles 6/7 (in μm^2) was counted manually and compared with the control and EGFP:FMRP (mean ± SE; n = 10–20 NMJs; one-way ANOVA). * $p<0.05$, ** $p<0.01$.
(PDF)

S2 Fig. FXS-causing mutations alter the liquid-like nature of SGs. Representative images of S2R+ cells transfected with GFP-FMRP mutants (green) and Rin-mCherry (red) that have been treated with 0.5mM sodium arsenite for 45 minutes followed by treatment with 10% 1,6-HD. Scale bars = 10μm. Note that both FMRP and Rin granules fail to dissipate in KH mutant cells relative to WT-FMRP controls.
(PDF)

S1 Table. Fly lines.
(DOCX)

S2 Table. Oligonucleotides.
(DOCX)

S3 Table. smFISH probes used for Fig 7.
(DOCX)

S4 Table. Raw data for statistical graphs used in all figures.
(XLSX)

Acknowledgments

We thank members of the S.A.B. lab for useful discussions. S2 cell lines and cDNAs were obtained from the *Drosophila* Genomics Resource Center. Fly lines were obtained from the Bloomington *Drosophila* Stock Center. We thank Samantha Patterson for assistance with FRAP experiments, Sarala Pradhan for help with developing and testing the FMRP translational reporter assay, and Navneeta Kaul for assistance constructing several of the *pAc5.1-FLuc 3'UTR* reporters. We are also grateful to the Knoebel Center for Healthy Aging for use of the ONI NanoImager for smFISH experiments.

Author Contributions

Conceptualization: Emily L. Starke, Scott A. Barbee.

Data curation: Emily L. Starke, Keelan Zius, Scott A. Barbee.

Formal analysis: Emily L. Starke, Keelan Zius, Scott A. Barbee.

Funding acquisition: Scott A. Barbee.

Investigation: Emily L. Starke, Keelan Zius.

Methodology: Emily L. Starke, Keelan Zius, Scott A. Barbee.

Project administration: Scott A. Barbee.

Resources: Scott A. Barbee.

Supervision: Scott A. Barbee.

Validation: Emily L. Starke, Keelan Zius.

Visualization: Emily L. Starke, Keelan Zius.

Writing – original draft: Emily L. Starke, Scott A. Barbee.

Writing – review & editing: Emily L. Starke, Keelan Zius, Scott A. Barbee.

References

1. Santoro MR, Bray SM, Warren ST. Molecular mechanisms of fragile X syndrome: a twenty-year perspective. Annu Rev Pathol. 2012; 7:219–45. Epub 20111010. https://doi.org/10.1146/annurev-pathol-011811-132457 PMID: 22017584.
2. Pieretti M, Zhang FP, Fu YH, Warren ST, Oostra BA, Caskey CT, et al. Absence of expression of the FMR-1 gene in fragile X syndrome. Cell. 1991; 66(4):817–22. Epub 1991/08/23. https://doi.org/10.1016/0092-8674(91)90125-i PMID: 1878973.
3. Richter JD, Zhao X. The molecular biology of FMRP: new insights into fragile X syndrome. Nat Rev Neurosci. 2021; 22(4):209–22. Epub 20210219. https://doi.org/10.1038/s41583-021-00432-0 PMID: 33608673; PubMed Central PMCID: PMC8094212.
4. Lai A, Valdez-Sinon AN, Bassell GJ. Regulation of RNA granules by FMRP and implications for neurological diseases. Traffic. 2020; 21(7):454–62. Epub 2020/05/07. https://doi.org/10.1111/tra.12733 PMID: 32374065; PubMed Central PMCID: PMC7377269.
5. Antar LN, Dictenberg JB, Plociniak M, Afroz R, Bassell GJ. Localization of FMRP-associated mRNA granules and requirement of microtubules for activity-dependent trafficking in hippocampal neurons. Genes Brain Behav. 2005; 4(6):350–9. Epub 2005/08/16. https://doi.org/10.1111/j.1601-183X.2005.00128.x PMID: 16098134.
6. Antar LN, Li C, Zhang H, Carroll RC, Bassell GJ. Local functions for FMRP in axon growth cone motility and activity-dependent regulation of filopodia and spine synapses. Mol Cell Neurosci. 2006; 32(1–2):37–48. Epub 20060502. https://doi.org/10.1016/j.mcn.2006.02.001 PMID: 16631377.
7. Dictenberg JB, Swanger SA, Antar LN, Singer RH, Bassell GJ. A direct role for FMRP in activity-dependent dendritic mRNA transport links filopodial-spine morphogenesis to fragile X syndrome. Dev Cell.

2008; 14(6):926–39. Epub 2008/06/10. https://doi.org/10.1016/j.devcel.2008.04.003 PMID: 18539120; PubMed Central PMCID: PMC2453222.

8. Li C, Bassell GJ, Sasaki Y. Fragile X Mental Retardation Protein is Involved in Protein Synthesis-Dependent Collapse of Growth Cones Induced by Semaphorin-3A. Front Neural Circuits. 2009; 3:11. Epub 20090915. https://doi.org/10.3389/neuro.04.011.2009 PMID: 19826618; PubMed Central PMCID: PMC2759364.

9. Banerjee A, Ifrim MF, Valdez AN, Raj N, Bassell GJ. Aberrant RNA translation in fragile X syndrome: From FMRP mechanisms to emerging therapeutic strategies. Brain Res. 2018; 1693(Pt A):24–36. Epub 20180410. https://doi.org/10.1016/j.brainres.2018.04.008 PMID: 29653083; PubMed Central PMCID: PMC7377270.

10. El Fatimy R, Davidovic L, Tremblay S, Jaglin X, Dury A, Robert C, et al. Tracking the Fragile X Mental Retardation Protein in a Highly Ordered Neuronal RiboNucleoParticles Population: A Link between Stalled Polyribosomes and RNA Granules. Plos Genet. 2016; 12(7):e1006192. Epub 20160727. https://doi.org/10.1371/journal.pgen.1006192 PMID: 27462983; PubMed Central PMCID: PMC4963131.

11. Banani SF, Lee HO, Hyman AA, Rosen MK. Biomolecular condensates: organizers of cellular biochemistry. Nat Rev Mol Cell Biol. 2017; 18(5):285–98. Epub 20170222. https://doi.org/10.1038/nrm.2017.7 PMID: 28225081; PubMed Central PMCID: PMC7434221.

12. Mittag T, Parker R. Multiple Modes of Protein-Protein Interactions Promote RNP Granule Assembly. J Mol Biol. 2018; 430(23):4636–49. Epub 20180809. https://doi.org/10.1016/j.jmb.2018.08.005 PMID: 30099026; PubMed Central PMCID: PMC6204294.

13. Van Treeck B, Parker R. Emerging Roles for Intermolecular RNA-RNA Interactions in RNP Assemblies. Cell. 2018; 174(4):791–802. Epub 2018/08/11. https://doi.org/10.1016/j.cell.2018.07.023 PMID: 30096311; PubMed Central PMCID: PMC6200146.

14. Tsang B, Arsenault J, Vernon RM, Lin H, Sonenberg N, Wang LY, et al. Phosphoregulated FMRP phase separation models activity-dependent translation through bidirectional control of mRNA granule formation. Proc Natl Acad Sci U S A. 2019; 116(10):4218–27. Epub 20190214. https://doi.org/10.1073/pnas.1814385116 PMID: 30765518; PubMed Central PMCID: PMC6410804.

15. Suhl JA, Warren ST. Single-Nucleotide Mutations in FMR1 Reveal Novel Functions and Regulatory Mechanisms of the Fragile X Syndrome Protein FMRP. J Exp Neurosci. 2015; 9(Suppl 2):35–41. Epub 20151208. https://doi.org/10.4137/JEN.S25524 PMID: 26819560; PubMed Central PMCID: PMC4720182.

16. De Boulle K, Verkerk AJ, Reyniers E, Vits L, Hendrickx J, Van Roy B, et al. A point mutation in the FMR-1 gene associated with fragile X mental retardation. Nat Genet. 1993; 3(1):31–5. Epub 1993/01/01. https://doi.org/10.1038/ng0193-31 PMID: 8490650.

17. Feng Y, Absher D, Eberhart DE, Brown V, Malter HE, Warren ST. FMRP associates with polyribosomes as an mRNP, and the I304N mutation of severe fragile X syndrome abolishes this association. Mol Cell. 1997; 1(1):109–18. Epub 1998/07/11. https://doi.org/10.1016/s1097-2765(00)80012-x PMID: 9659908

18. Zang JB, Nosyreva ED, Spencer CM, Volk LJ, Musunuru K, Zhong R, et al. A mouse model of the human Fragile X syndrome I304N mutation. Plos Genet. 2009; 5(12):e1000758. Epub 20091211. https://doi.org/10.1371/journal.pgen.1000758 PMID: 20011099; PubMed Central PMCID: PMC2779495.

19. Myrick LK, Deng PY, Hashimoto H, Oh YM, Cho Y, Poidevin MJ, et al. Independent role for presynaptic FMRP revealed by an FMR1 missense mutation associated with intellectual disability and seizures. Proc Natl Acad Sci U S A. 2015; 112(4):949–56. Epub 20150105. https://doi.org/10.1073/pnas.1423094112 PMID: 25561520; PubMed Central PMCID: PMC4313821.

20. Myrick LK, Hashimoto H, Cheng X, Warren ST. Human FMRP contains an integral tandem Agenet (Tudor) and KH motif in the amino terminal domain. Hum Mol Genet. 2015; 24(6):1733–40. Epub 20141120. https://doi.org/10.1093/hmg/ddu586 PMID: 25416280; PubMed Central PMCID: PMC4381759.

21. Prieto M, Folci A, Poupon G, Schiavi S, Buzzelli V, Pronot M, et al. Missense mutation of Fmr1 results in impaired AMPAR-mediated plasticity and socio-cognitive deficits in mice. Nat Commun. 2021; 12(1):1557. Epub 20210310. https://doi.org/10.1038/s41467-021-21820-1 PMID: 33692361; PubMed Central PMCID: PMC7946954.

22. Darnell JC, Fraser CE, Mostovetsky O, Stefani G, Jones TA, Eddy SR, et al. Kissing complex RNAs mediate interaction between the Fragile-X mental retardation protein KH2 domain and brain polyribosomes. Genes Dev. 2005; 19(8):903–18. Epub 20050401. https://doi.org/10.1101/gad.1276805 PMID: 15805463; PubMed Central PMCID: PMC1080130.

23. Ascano M Jr., Mukherjee N, Bandaru P, Miller JB, Nusbaum JD, Corcoran DL, et al. FMRP targets distinct mRNA sequence elements to regulate protein expression. Nature. 2012; 492(7429):382–6. Epub

20121212. https://doi.org/10.1038/nature11737 PMID: 23235829; PubMed Central PMCID: PMC3528815.

24. Ray D, Kazan H, Cook KB, Weirauch MT, Najafabadi HS, Li X, et al. A compendium of RNA-binding motifs for decoding gene regulation. Nature. 2013; 499(7457):172–7. Epub 2013/07/13. https://doi.org/10.1038/nature12311 PMID: 23846655; PubMed Central PMCID: PMC3929597.

25. Suhl JA, Chopra P, Anderson BR, Bassell GJ, Warren ST. Analysis of FMRP mRNA target datasets reveals highly associated mRNAs mediated by G-quadruplex structures formed via clustered WGGA sequences. Hum Mol Genet. 2014; 23(20):5479–91. Epub 20140529. https://doi.org/10.1093/hmg/ddu272 PMID: 24876161; PubMed Central PMCID: PMC4168832.

26. Myrick LK, Nakamoto-Kinoshita M, Lindor NM, Kirmani S, Cheng X, Warren ST. Fragile X syndrome due to a missense mutation. Eur J Hum Genet. 2014; 22(10):1185–9. Epub 20140122. https://doi.org/10.1038/ejhg.2013.311 PMID: 24448548; PubMed Central PMCID: PMC4169535.

27. Agulhon C, Blanchet P, Kobetz A, Marchant D, Faucon N, Sarda P, et al. Expression of FMR1, FXR1, and FXR2 genes in human prenatal tissues. J Neuropathol Exp Neurol. 1999; 58(8):867–80. Epub 1999/08/14. https://doi.org/10.1097/00005072-199908000-00009 PMID: 10446811.

28. Zhang Y, O'Connor JP, Siomi MC, Srinivasan S, Dutra A, Nussbaum RL, et al. The fragile X mental retardation syndrome protein interacts with novel homologs FXR1 and FXR2. Embo J. 1995; 14(21):5358–66. Epub 1995/11/01. PMID: 7489725; PubMed Central PMCID: PMC394645.

29. Wan L, Dockendorff TC, Jongens TA, Dreyfuss G. Characterization of dFMR1, a Drosophila melanogaster homolog of the fragile X mental retardation protein. Mol Cell Biol. 2000; 20(22):8536–47. Epub 2000/10/25. https://doi.org/10.1128/MCB.20.22.8536-8547.2000 PMID: 11046149; PubMed Central PMCID: PMC102159.

30. Barbee SA, Estes PS, Cziko AM, Hillebrand J, Luedeman RA, Coller JM, et al. Staufen- and FMRP-containing neuronal RNPs are structurally and functionally related to somatic P bodies. Neuron. 2006; 52(6):997–1009. Epub 2006/12/21. https://doi.org/10.1016/j.neuron.2006.10.028 PMID: 17178403; PubMed Central PMCID: PMC1955741.

31. Cougot N, Bhattacharyya SN, Tapia-Arancibia L, Bordonne R, Filipowicz W, Bertrand E, et al. Dendrites of mammalian neurons contain specialized P-body-like structures that respond to neuronal activation. J Neurosci. 2008; 28(51):13793–804. Epub 2008/12/19. https://doi.org/10.1523/JNEUROSCI.4155-08.2008 PMID: 19091970; PubMed Central PMCID: PMC6671906.

32. Drozd M, Bardoni B, Capovilla M. Modeling Fragile X Syndrome in Drosophila. Front Mol Neurosci. 2018; 11:124. Epub 20180416. https://doi.org/10.3389/fnmol.2018.00124 PMID: 29713264; PubMed Central PMCID: PMC5911982.

33. Zhang YQ, Bailey AM, Matthies HJ, Renden RB, Smith MA, Speese SD, et al. Drosophila fragile X-related gene regulates the MAP1B homolog Futsch to control synaptic structure and function. Cell. 2001; 107(5):591–603. Epub 2001/12/06. https://doi.org/10.1016/s0092-8674(01)00589-x PMID: 11733059.

34. Gareau C, Houssin E, Martel D, Coudert L, Mellaoui S, Huot ME, et al. Characterization of fragile X mental retardation protein recruitment and dynamics in Drosophila stress granules. PLoS One. 2013; 8(2):e55342. Epub 20130207. https://doi.org/10.1371/journal.pone.0055342 PMID: 23408971; PubMed Central PMCID: PMC3567066.

35. Gareau C, Martel D, Coudert L, Mellaoui S, Mazroui R. Characterization of Fragile X Mental Retardation Protein granules formation and dynamics in Drosophila. Biol Open. 2013; 2(1):68–81. Epub 20121031. https://doi.org/10.1242/bio.20123012 PMID: 23336078; PubMed Central PMCID: PMC3545270.

36. Valverde R, Pozdnyakova I, Kajander T, Venkatraman J, Regan L. Fragile X mental retardation syndrome: structure of the KH1-KH2 domains of fragile X mental retardation protein. Structure. 2007; 15(9):1090–8. Epub 2007/09/14. https://doi.org/10.1016/j.str.2007.06.022 PMID: 17850748.

37. Shin Y, Brangwynne CP. Liquid phase condensation in cell physiology and disease. Science. 2017; 357(6357). Epub 2017/09/25. https://doi.org/10.1126/science.aaf4382 PMID: 28935776.

38. Tourriere H, Chebli K, Zekri L, Courselaud B, Blanchard JM, Bertrand E, et al. The RasGAP-associated endoribonuclease G3BP assembles stress granules. J Cell Biol. 2003; 160(6):823–31. Epub 2003/03/19. https://doi.org/10.1083/jcb.200212128 PMID: 12642610; PubMed Central PMCID: PMC2173781.

39. Kroschwald S, Maharana S, Simon A. Hexanediol: a chemical probe to investigate the material properties of membrane-less compartments. Matters. 2017. https://doi.org/10.19185/matters.201702000010

40. Kim SH, Dong WK, Weiler IJ, Greenough WT. Fragile X mental retardation protein shifts between polyribosomes and stress granules after neuronal injury by arsenite stress or in vivo hippocampal electrode insertion. J Neurosci. 2006; 26(9):2413–8. https://doi.org/10.1523/JNEUROSCI.3680-05.2006 PMID: 16510718; PubMed Central PMCID: PMC6793656.

41. Coller J, Parker R. General translational repression by activators of mRNA decapping. Cell. 2005; 122 (6):875–86. https://doi.org/10.1016/j.cell.2005.07.012 PMID: 16179257; PubMed Central PMCID: PMC1853273.

42. Pradhan SJ, Nesler KR, Rosen SF, Kato Y, Nakamura A, Ramaswami M, et al. The conserved P body component HPat/Pat1 negatively regulates synaptic terminal growth at the larval Drosophila neuromuscular junction. J Cell Sci. 2012; 125(Pt 24):6105–16. Epub 20121024. https://doi.org/10.1242/jcs.113043 PMID: 23097047; PubMed Central PMCID: PMC3585522.

43. Antar LN, Afroz R, Dictenberg JB, Carroll RC, Bassell GJ. Metabotropic glutamate receptor activation regulates fragile x mental retardation protein and FMR1 mRNA localization differentially in dendrites and at synapses. J Neurosci. 2004; 24(11):2648–55. https://doi.org/10.1523/JNEUROSCI.0099-04.2004 PMID: 15028757; PubMed Central PMCID: PMC6729525.

44. Davidovic L, Jaglin XH, Lepagnol-Bestel AM, Tremblay S, Simonneau M, Bardoni B, et al. The fragile X mental retardation protein is a molecular adaptor between the neurospecific KIF3C kinesin and dendritic RNA granules. Hum Mol Genet. 2007; 16(24):3047–58. Epub 20070919. https://doi.org/10.1093/hmg/ddm263 PMID: 17881655.

45. Morales J, Hiesinger PR, Schroeder AJ, Kume K, Verstreken P, Jackson FR, et al. Drosophila fragile X protein, DFXR, regulates neuronal morphology and function in the brain. Neuron. 2002; 34(6):961–72. https://doi.org/10.1016/s0896-6273(02)00731-6 PMID: 12086643.

46. Estes PS, O'Shea M, Clasen S, Zarnescu DC. Fragile X protein controls the efficacy of mRNA transport in Drosophila neurons. Mol Cell Neurosci. 2008; 39(2):170–9. Epub 20080628. https://doi.org/10.1016/j.mcn.2008.06.012 PMID: 18655836.

47. Chen E, Sharma MR, Shi X, Agrawal RK, Joseph S. Fragile X mental retardation protein regulates translation by binding directly to the ribosome. Mol Cell. 2014; 54(3):407–17. Epub 20140417. https://doi.org/10.1016/j.molcel.2014.03.023 PMID: 24746697; PubMed Central PMCID: PMC4019695.

48. Xu K, Bogert BA, Li W, Su K, Lee A, Gao FB. The fragile X-related gene affects the crawling behavior of Drosophila larvae by regulating the mRNA level of the DEG/ENaC protein pickpocket1. Curr Biol. 2004; 14(12):1025–34. Epub 2004/06/19. https://doi.org/10.1016/j.cub.2004.05.055 PMID: 15202995.

49. Sudhakaran IP, Hillebrand J, Dervan A, Das S, Holohan EE, Hulsmeier J, et al. FMRP and Ataxin-2 function together in long-term olfactory habituation and neuronal translational control. Proc Natl Acad Sci U S A. 2014; 111(1):E99–E108. Epub 20131216. https://doi.org/10.1073/pnas.1309543111 PMID: 24344294; PubMed Central PMCID: PMC3890871.

50. Reeve SP, Bassetto L, Genova GK, Kleyner Y, Leyssen M, Jackson FR, et al. The Drosophila fragile X mental retardation protein controls actin dynamics by directly regulating profilin in the brain. Curr Biol. 2005; 15(12):1156–63. Epub 2005/06/21. https://doi.org/10.1016/j.cub.2005.05.050 PMID: 15964283.

51. Formicola N, Vijayakumar J, Besse F. Neuronal ribonucleoprotein granules: Dynamic sensors of localized signals. Traffic. 2019; 20(9):639–49. Epub 20190729. https://doi.org/10.1111/tra.12672 PMID: 31206920.

52. Davis JK, Broadie K. Multifarious Functions of the Fragile X Mental Retardation Protein. Trends Genet. 2017; 33(10):703–14. Epub 20170818. https://doi.org/10.1016/j.tig.2017.07.008 PMID: 28826631; PubMed Central PMCID: PMC5610095.

53. Adinolfi S, Ramos A, Martin SR, Dal Piaz F, Pucci P, Bardoni B, et al. The N-terminus of the fragile X mental retardation protein contains a novel domain involved in dimerization and RNA binding. Biochemistry. 2003; 42(35):10437–44. https://doi.org/10.1021/bi034909g PMID: 12950170.

54. Kim TH, Tsang B, Vernon RM, Sonenberg N, Kay LE, Forman-Kay JD. Phospho-dependent phase separation of FMRP and CAPRIN1 recapitulates regulation of translation and deadenylation. Science. 2019; 365(6455):825–9. Epub 2019/08/24. https://doi.org/10.1126/science.aax4240 PMID: 31439799.

55. Banani SF, Rice AM, Peeples WB, Lin Y, Jain S, Parker R, et al. Compositional Control of Phase-Separated Cellular Bodies. Cell. 2016; 166(3):651–63. Epub 20160630. https://doi.org/10.1016/j.cell.2016.06.010 PMID: 27374333; PubMed Central PMCID: PMC4967043.

56. Li P, Banjade S, Cheng HC, Kim S, Chen B, Guo L, et al. Phase transitions in the assembly of multivalent signalling proteins. Nature. 2012; 483(7389):336–40. Epub 20120307. https://doi.org/10.1038/nature10879 PMID: 22398450; PubMed Central PMCID: PMC3343696.

57. Vijayakumar J, Perrois C, Heim M, Bousset L, Alberti S, Besse F. The prion-like domain of Drosophila Imp promotes axonal transport of RNP granules in vivo. Nat Commun. 2019; 10(1):2593. Epub 20190613. https://doi.org/10.1038/s41467-019-10554-w PMID: 31197139; PubMed Central PMCID: PMC6565635.

58. Gopal PP, Nirschl JJ, Klinman E, Holzbaur EL. Amyotrophic lateral sclerosis-linked mutations increase the viscosity of liquid-like TDP-43 RNP granules in neurons. Proc Natl Acad Sci U S A. 2017; 114(12):E2466–E75. Epub 20170306. https://doi.org/10.1073/pnas.1614462114 PMID: 28265061; PubMed Central PMCID: PMC5373408.

59. Chae YS, Lee SH, Cheang YH, Lee N, Rim YS, Jang DJ, et al. Neuronal RNA granule contains ApC-PEB1, a novel cytoplasmic polyadenylation element binding protein, in Aplysia sensory neuron. Exp Mol Med. 2010; 42(1):30–7. Epub 2009/11/06. https://doi.org/10.3858/emm.2010.42.1.003 PMID: 19887896; PubMed Central PMCID: PMC2811818.

60. Athar YM, Joseph S. RNA-Binding Specificity of the Human Fragile X Mental Retardation Protein. J Mol Biol. 2020; 432(13):3851–68. Epub 20200425. https://doi.org/10.1016/j.jmb.2020.04.021 PMID: 32343993; PubMed Central PMCID: PMC7306444.

61. Molliex A, Temirov J, Lee J, Coughlin M, Kanagaraj AP, Kim HJ, et al. Phase separation by low complexity domains promotes stress granule assembly and drives pathological fibrillization. Cell. 2015; 163 (1):123–33. Epub 2015/09/26. https://doi.org/10.1016/j.cell.2015.09.015 PMID: 26406374; PubMed Central PMCID: PMC5149108.

62. Schwartz JC, Wang X, Podell ER, Cech TR. RNA seeds higher-order assembly of FUS protein. Cell Rep. 2013; 5(4):918–25. Epub 20131121. https://doi.org/10.1016/j.celrep.2013.11.017 PMID: 24268778; PubMed Central PMCID: PMC3925748.

63. Ishizuka A, Siomi MC, Siomi H. A Drosophila fragile X protein interacts with components of RNAi and ribosomal proteins. Genes Dev. 2002; 16(19):2497–508. https://doi.org/10.1101/gad.1022002 PMID: 12368261; PubMed Central PMCID: PMC187455.

64. Darnell JC, Van Driesche SJ, Zhang C, Hung KY, Mele A, Fraser CE, et al. FMRP stalls ribosomal translocation on mRNAs linked to synaptic function and autism. Cell. 2011; 146(2):247–61. Epub 2011/07/26. https://doi.org/10.1016/j.cell.2011.06.013 PMID: 21784246; PubMed Central PMCID: PMC3232425.

65. Goering R, Hudish LI, Guzman BB, Raj N, Bassell GJ, Russ HA, et al. FMRP promotes RNA localization to neuronal projections through interactions between its RGG domain and G-quadruplex RNA sequences. Elife. 2020;9. Epub 20200608. https://doi.org/10.7554/eLife.52621 PMID: 32510328; PubMed Central PMCID: PMC7279889.

66. Darnell JC, Fraser CE, Mostovetsky O, Darnell RB. Discrimination of common and unique RNA-binding activities among Fragile X mental retardation protein paralogs. Hum Mol Genet. 2009; 18(17):3164–77. Epub 20090601. https://doi.org/10.1093/hmg/ddp255 PMID: 19487368; PubMed Central PMCID: PMC2722981.

67. Patel A, Lee HO, Jawerth L, Maharana S, Jahnel M, Hein MY, et al. A Liquid-to-Solid Phase Transition of the ALS Protein FUS Accelerated by Disease Mutation. Cell. 2015; 162(5):1066–77. Epub 2015/09/01. https://doi.org/10.1016/j.cell.2015.07.047 PMID: 26317470.

68. Behm-Ansmant I, Rehwinkel J, Doerks T, Stark A, Bork P, Izaurralde E. mRNA degradation by miRNAs and GW182 requires both CCR4:NOT deadenylase and DCP1:DCP2 decapping complexes. Genes Dev. 2006; 20(14):1885–98. Epub 20060630. https://doi.org/10.1101/gad.1424106 PMID: 16815998; PubMed Central PMCID: PMC1522082.

69. Nesler KR, Sand RI, Symmes BA, Pradhan SJ, Boin NG, Laun AE, et al. The miRNA pathway controls rapid changes in activity-dependent synaptic structure at the Drosophila melanogaster neuromuscular junction. PLoS One. 2013; 8(7):e68385. Epub 20130702. https://doi.org/10.1371/journal.pone.0068385 PMID: 23844193; PubMed Central PMCID: PMC3699548.

70. Cheney PP, Weisgerber AW, Feuerbach AM, Knowles MK. Single Lipid Molecule Dynamics on Supported Lipid Bilayers with Membrane Curvature. Membranes (Basel). 2017; 7(1). Epub 20170315. https://doi.org/10.3390/membranes7010015 PMID: 28294967; PubMed Central PMCID: PMC5371976.

71. Bolte S, Cordelieres FP. A guided tour into subcellular colocalization analysis in light microscopy. J Microsc. 2006; 224(Pt 3):213–32. Epub 2007/01/11. https://doi.org/10.1111/j.1365-2818.2006.01706.x PMID: 17210054.

72. Basu H, Ding L, Pekkurnaz G, Cronin M, Schwarz TL. Kymolyzer, a Semi-Autonomous Kymography Tool to Analyze Intracellular Motility. Curr Protoc Cell Biol. 2020; 87(1):e107. Epub 2020/06/13. https://doi.org/10.1002/cpcb.107 PMID: 32530579.

73. Mueller F, Senecal A, Tantale K, Marie-Nelly H, Ly N, Collin O, et al. FISH-quant: automatic counting of transcripts in 3D FISH images. Nat Methods. 2013; 10(4):277–8. Epub 2013/03/30. https://doi.org/10.1038/nmeth.2406 PMID: 23538861.

74. Erdos G, Dosztanyi Z. Analyzing Protein Disorder with IUPred2A. Curr Protoc Bioinformatics. 2020; 70 (1):e99. Epub 2020/04/03. https://doi.org/10.1002/cpbi.99 PMID: 32237272.